Coversheet/Statement

Title: “**Tectonostratigraphy of the Late Neoproterozoic in the Eastern Arabian Plate – a revision of the Ediacaran geological evolution in the Central Oman Mountains (Jabal Al Akhdar, Sultanate of Oman)**”

Authors:
Ivan Callegari[1*](ivan.callegari@gutech.edu.om)
Andreas Scharf[2](scharfa@squ.edu.om)
Andre F. Pinto[3](jorgeandre@uniovi.es)
Frank Mattern[2](fmattern@zedat.fu-berlin.de)
Rajat Mazumder[1](rajat.mazumder@gutech.edu.om)
Debasmita Datta[4] (dattadebasmita@iitgn.ac.in)
Heninjara Rarivoarison[1](h.rarivoarison@gutech.edu.om)

[1] Department of Applied Geosciences, German University of Technology GUtech, P.O. Box: 1816, PC 130, Halban, Sultanate of Oman
[2] Department of Earth Sciences, College of Science, Sultan Qaboos University, P.O. Box: 36, PC 123, Al-Khoud, Muscat, Sultanate of Oman
[3] Department of Geology, Faculty of Sciences, University of Oviedo, C/ Jesús Arias de Velasco, s/n, 33009 Oviedo, Spain
[4] Department of Earth Sciences, Indian Institute of Technology Gandhinagar, Gujarat-382355, India

*Corresponding author

The paper is a non-peer reviewed preprint submitted to EarthArXiv. The preprint it was submitted to the Geological Society of London (Special Publication) for peer review and it is still under review.

Full title: Tectonostratigraphy of the Late Neoproterozoic in the Eastern Arabian Plate – a revision of the Ediacaran geological evolution in the Central Oman Mountains (Jabal Al Akhdar, Sultanate of Oman)

Abbreviated title: Late Neoproterozoic in Eastern Arabian Plate

Ivan Callegari[1*], Andreas Scharf[2], Andre F. Pinto[3], Frank Mattern[2], Rajat Mazumder[1], Debasmita Datta[4] and Heninjara Rarivoarison[1].

[1] Department of Applied Geosciences, German University of Technology GUtech, P.O. Box: 1816, PC 130, Halban, Sultanate of Oman

[2] Department of Earth Sciences, College of Science, Sultan Qaboos University, P.O. Box: 36, PC 123, Al-Khoud, Muscat, Sultanate of Oman

[3] Department of Geology, Faculty of Sciences, University of Oviedo, C/ Jesús Arias de Velasco, s/n, 33009 Oviedo, Spain

[4] Department of Earth Sciences, Indian Institute of Technology Gandhinagar, Gujarat-382355, India

*Corresponding author

ABSTRACT

In northeastern Oman, within the Neoproterozoic Huqf Supergroup, well-exposed sedimentary formations spanning the Cryogenian to Ediacaran periods, lie beneath the late Palaeozoic "Hercynian Unconformity". These rocks bear the marks of the distant Cadomian Orogeny. Among these, the youngest correspond to the diverse Ediacaran Fara Formation, a member of the Ara Group. Our study extensively examined Fara Formation's lithologies, stratigraphy, and syndepositional deformation features to shed light on the Neoproterozoic geological evolution of eastern Arabia. Through meticulous analysis, several key findings emerged from our investigation: (1)Fara Formation can be categorized into three distinct members (FA1-FA3); (2) while FA1 and FA2 show signs of Cadomian D1 deformation, FA3 conceals these deformed layers with an angular unconformity; (3) the entire Fara Formation is of Ediacaran age, dating back over 538 million years; (4) the volcaniclastic rocks within Fara Formation are geochemically similar to Hormuz´s volcanics from the same period ; (5) carbonates and siliciclastic rocks of FA1 and FA2 formed within a NW-SE striking back-arc basin associated with Cadomian deformation, while FA3's shallow-marine siliciclastic rocks unconformably overlie the latter members, and (6) Fara Formation documents the deepening of a stable carbonate platform, reflecting a major event in the geological history of Eastern Arabia.

KEYWORDS: Active continental margin, Back-arc basin, Cadomian, Angudan, *Palaeopascichnus*

INTRODUCTION

The Neoproterozoic Era is a geological time interval characterized by significant changes in terms of climate, biological and tectonic evolution. These last were brought about alongside the formation and breakup of the supercontinent Rodinia, as well as the first stage of the assembly of Gondwana, from ca. 730 Ma to ca. 500 Ma. This process culminated in the collision of East and West Gondwana to form the Pan-African orogeny (Mallard and Rogers, 1997; Veevers, 2004, Xiao and Kaufman, 2006, Thomson et al., 2015). In this era, extensive glaciations occurred in tandem with the development of metazoan multicellular animals; a major milestone of the Earth systems' history (Xiao and Kaufman, 2006).

In this work, we revise the tectonostratigraphy of the Late Ediacaran lithologies in Eastern Arabia. More specifically, Ediacaran outcrops in Oman are sparse and restricted to the cores of the Jabal Akhdar and Saih Hatat domes of the Oman Mountains (Fig. 1), and to the Huqf and Salalah areas in Central and South Oman, respectively. Ediacaran rocks are present also in the subsurface of Oman, and they have been the subject of geophysical and well studies due to their potential for hosting hydrocarbons (e.g., Amthor et al., 2005; Schröder and Grotzinger, 2007; Forbes et al., 2010; Cozzi et al., 2012; Grotzinger and Al-Rawahi, 2014; Osburn et al., 2014). The excellent outcrop conditions of the Ediacaran rocks in the Jabal Akhdar Dome and the fact that these rocks were only moderately deformed during the Late Cretaceous plate convergence, make them a prime target to study the stratigraphy and tectonic evolution of the Neoproterozoic. The Late Ediacaran has been described by Allen (2007) in the context of a passive margin, eventually becoming active at the top of the sequence.

This article intends to contribute significantly to the causal understanding of sedimentation, volcanism, and tectonics of the eastern Arabian Plate, through stratigraphic, structural, and petrological investigations, focusing on the associated time constraints and the significance of angular unconformities. At the same time, we investigated new and excellent outcrops, which enabled further detailed observations. A rare fossil of a skeletal macroscopic organism from the upper part of Late Ediacaran Fara Formation is also here presented and discussed for the first time. Finally, the present work´s detailed and revised stratigraphy/lithostratigraphy of the Fara Formation, alongside geochemical analyses of volcanogenic rocks provide new insights on the Neoproterozoic geological evolution of Eastern Arabia.

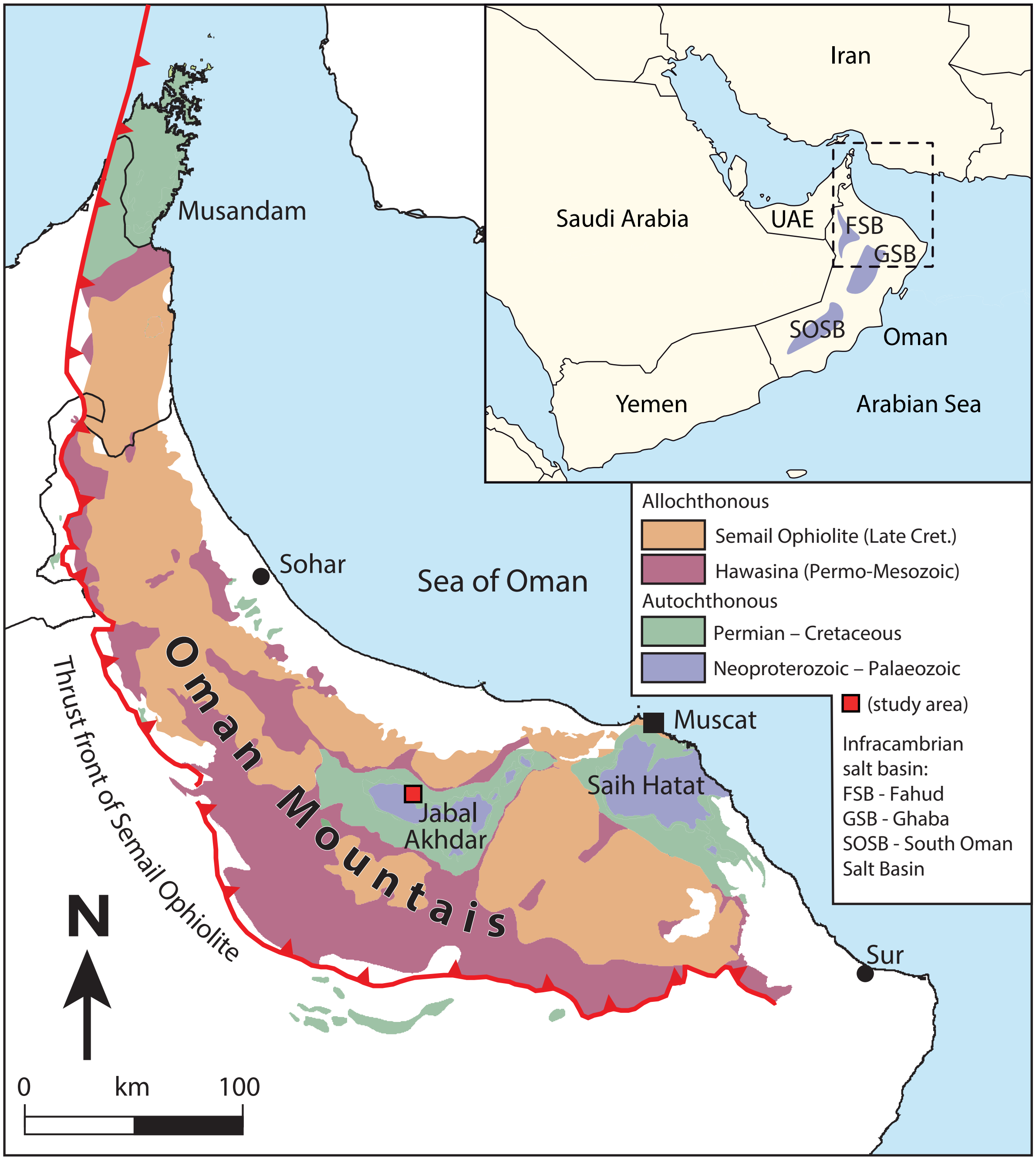

Figure 1. Geological overview map of the north-eastern Arabian Peninsula. Map modified after (Forbes et al., 2010). Parts of the northern Oman Mountains are drawn after the geological map from the United Arab Emirates (UAE) (Styles et al., 2006). FSB-Fahud, GSB-Ghaba and SOSB-South Oman Salt Basin: Infracambrian salt basins.

GEOLOGICAL SETTING

The Oman Mountains contain a complex assemblage of Neoproterozoic to Neogene mostly siliciclastic rocks and carbonates, with the Neoproterozoic lithologies exposed in the cores of the Jabal Akhdar and Saih Hatat domes (Fig. 1; e.g., Béchennec et al., 1992). While the eastern Saih Hatat area was intensely affected by continental subduction during the Late Cretaceous, the Jabal Akhdar region was only shallowly dragged into the respective subduction zone, displaying mostly sub-greenschist facies conditions (e.g., Breton et al., 2004; Agard et al., 2010; Hansman et al., 2021) or possibly blueschist-facies conditions (Zuccari et al., 2023). Thus, the Ediacaran rocks of the Jabal Akhdar Dome preserved the original pre-subduction deformation structures (Callegari et al., 2020).

The oldest formation of the Jabal Akhdar Dome is the siliciclastic >1500-m-thick Mistal Formation (subsurface equivalent is the Abu Mahara Group and Masirah Bay Formation), consisting of an alternation of siltstones, sandstones and diamictites (Beurrier et al., 1986). The lower section of the Mistal Formation contains tuffaceous beds, which yield U-Pb zircon ages of ~720 Ma (Brasier et al., 2000; Bowring et al., 2007; Allen et al., 2011). The top of this formation has an age of ~635 Ma, marking the boundary between the Cryogenian and the Ediacaran (e.g., Allen and Leather, 2006; Allen et al., 2011). The next and younger Ediacaran Hajir or Khufai Formation (subsurface name) comprises dark carbonates with stromatolites, and yields <100 m of thickness (Beurrier et al., 1986). This formation is followed by the siliciclastic Mu'aydin or Shuram Formation (subsurface name) with a thickness of 800 m (Beurrier et al., 1986; Mattern and Scharf, 2019). Above Mu'aydin Formation, limestones and dolostones of the Kharus or Buah Formation (subsurface name) follows, with a thickness of <245 m.

The youngest Neoproterozoic to earliest Cambrian(?) formation within Jabal Akhdar Dome is Fara Formation, with a thickness of ~380 m (Beurrier et al., 1986). This formation encompasses diverse lithologies, including carbonates, cherts, volcaniclastic rocks, siltstones, sandstones, and conglomerates (Beurrier et al., 1986). The Fara Formation overlies Kharus Formation conformably (Béchennec et al., 1992) and is itself overlain by the Upper Permian Saiq Formation at an angular unconformity. This "Hercynian Unconformity" separates the Saiq or Khuff Formation (subsurface name) from the various underlying Neoproterozoic formations (Fig. 2). More details on the pre-Permian stratigraphy and tectonics of the Jabal Akhdar Dome are provided in Scharf et al. (2021b, c).

The age of the Fara Formation is correlated to Ara Group´s and presumed to be of Neoproterozoic (Beurrier et al., 1986) to earliest Cambrian age (Bowring et al., 2007; Forbes et al., 2010 and references therein). The lithologies of Fara Formation in the Jabal Akhdar Dome differs from the supposed age-equivalent subsurface rocks from the interior and southern Oman.

The Ara Group in the subsurface is characterized by a carbonate-evaporite sequence (FSB, GSB and SOSB, respectively Fahud Salt Basin, Ghaba Salt Basin, and South Oman Salt Basin in Fig. 1) with thick salt deposits (e.g., Mattes and Conway-Morris, 1990) which accumulated in a transpressional/transtensional basin setting (Forbes et al., 2010 and references therein). Some shale and silica-rich sedimentary deposits (silicilyte in Amthor et al., 2005 and Stolper et al., 2017) occur in the South Oman Salt Basin (e.g., Amthor et al., 2005). The thick Ara evaporites were deposited in geographically confiend and NNE/SSW-striking basins (i.e., South Oman Salt Basin, Ghaba Salt Basin) during periods of low relative sea level, where stratified, anoxic conditions periodically prevailed and organic-rich sediments and salt were deposited (e.g., Mattes and Conway-Morris, 1990; Edgell, 1991). The silicilyte formed at times of low siliciclastic input in reducing, possible anoxic intra-cratonic basins below wave base at a depth of >~100-200 m (Amthor et al., 2005; Stolper et al., 2017). The rocks of the subsurface Ara Group record the segmentation of the regionally extensive Nafun Basin into three smaller units, represented by the subsurface salt basins in Oman (Fahud-, Ghaba- and South Oman Salt basins). The carbonate–evaporite succession of the Ara Group in the South Oman Salt Basin (Schröder et al., 2003) is the potential age-equivalent of a peritidal carbonate succession in the Huqf area (Nicholas and Brasier, 2000), and Fara Formation of the Jabal Akhdar Dome (Rieu et al., 2007).

The Neoproterozoic formations of the Jabal Akhdar Dome were affected by two pre-Permian deformation events (D1 and D2 in Callegari et al., 2020). The first (D1) generated ~NW/SE-oriented folds, refolded by a second deformation event (D2) that produced NE/SW-oriented folds (Callegari et al., 2020; Scharf et al., 2021a). The D1 interval is related to the Cadomian Orogeny (Callegari et al., 2020; Scharf et al., 2021a). The D2 episode is related to the contractional Angudan event at 525 ±5 Ma (Droste, 2014), which ensued after deposition of the upper member of Fara Formation. The D2 event is marked by the Angudan Unconformity, coinciding with the final stage of the East African Orogeny (~550–510 Ma; Loosveld et al., 1996; Al-Husseini, 2000; Immerz et al., 2000; Koopman et al., 2007; Forbes et al., 2010; Al-Kindi and Richard, 2014; Droste, 2014).

An early Palaeozoic rifting interval produced accommodation space for the deposition of the ~3 km thick Cambro-Ordovician Amdeh Formation (Lovelock et al., 1981; Oterdoom et al., 1999; Heward et al., 2018). However, the siliciclastics of the latter formation are only exposed east of the Jabal Akhdar Dome and there is no evidence of the presence of these rocks in the Jabal Akhdar area (e.g., Mattern et al., 2018).

Arabia was affected by large-scale arch formation during the Late Palaeozoic (Faqira et al., 2009), resulting in the widespread "Hercynian Unconformity" (e.g., Glennie et al., 1974). Above this angular unconformity, the Permian Saiq Formation, consisting of a basal conglomerate and a thick carbonate succession, accumulated in the future Jabal Akhdar region (Béchennec at al., 1992) while the late Palaeozoic rifting of Pangea affected northeastern Oman (e.g., Blendinger et al., 1990; Chauvet et al., 2009). Following the latter event, seafloor spreading led to formation of the Neo-Tethys Ocean and the Hawasina deep-sea basin NE of Oman (e.g., Glennie et al., 1974). During the Cenomanian, another spreading centre within the Neo-Tethys Ocean produced new oceanic lithosphere, corresponding to the future Semail Ophiolite (e.g., Tilton et al., 1981;

Stampfli and Borel, 2002). Coeval with its formation, the Neo-Tethys lithosphere was subducted towards the NE, while the Semail Ophiolite was thrust towards the SW, at first above the oceanic lithosphere of the Neo-Tethys (e.g., Tilton et al., 1981; Rioux et al., 2016) and eventually overlying the continental Arabian lithosphere of the Hawasina Basin and Arabian margin. The ophiolite emplacement was completed at ~75 Ma (Searle, 2007) and the autochthonous rocks of the future Jabal Akhdar area were dragged into the subduction zone during the Late Cretaceous (Breton et al., 2004; Zuccari et al., 2023). Posteriorly, the Arabian lithosphere was exhumed from the subduction zone (e.g., Breton et al., 2004; Al-Wardi and Butler, 2007; Grobe et al., 2018, 2019; Scharf et al., 2019). This exhumation correlates with extensional shearing and exhumation of the Saih Hatat Dome lasting from the latest Cretaceous until the early Eocene (e.g., Hansman et al., 2017). During the same period little to no exhumation of the Jabal Akhdar Dome occurred (Hansman et al., 2017). This changed during the late Eocene, when the surface uplift of the Jabal Akhdar Dome amounted to 4-6 km (Hansman et al., 2017), forming the broad anticline of the Jabal Akhdar Dome. Doming resulted in a NE-ward tilting with ~20° of the units exposed in Wadi Bani Awf, including rocks of the Kharus and Fara formations (Beurrier et al., 1986).

Review of the Kharus (Buah) and Fara formations

In Wadi Bani Awf of the Jabal Akhdar Dome, deposition of the Kharus Formation preceded that of Fara Formation (Fig. 2). The Kharus Formation was deposited in a tidal flat environment (Beurrier et al., 1986) and is characterized by stromatolite-bearing carbonates, showing an upward-shoaling trend from sub-wave base to sabkha deposits.

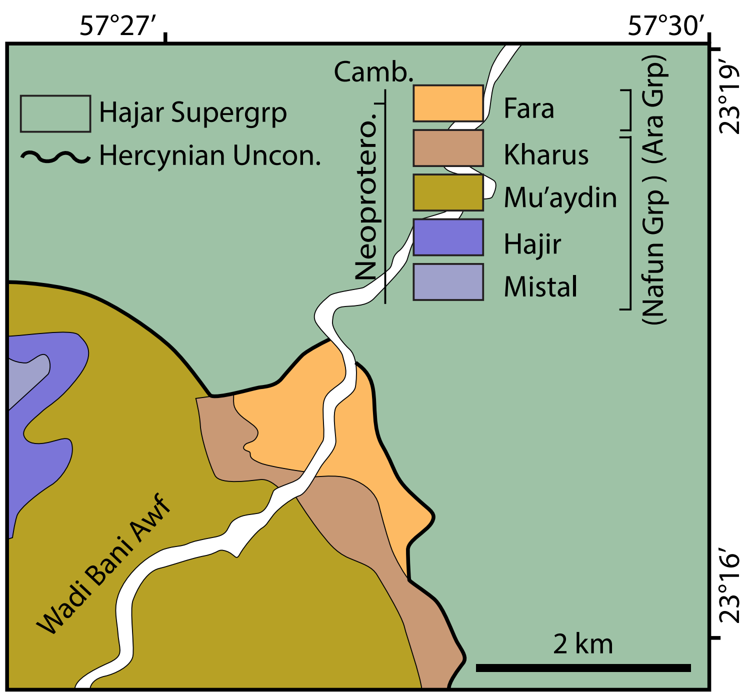

Figure 2. Simplified geological map of Wadi Bani Awf after Beurrier et al. (1986). Note that the age of Fara Formation is assumed to be Ediacaran and earliest Cambrian (Beurrier et al., 1986).

The upper part contains slump features and brecciated beds of a ramp slope, with thick breccia units representing slope failure deposits (Mc Carron, 1999). El-Ghali et al. (2020) dated carbonate samples collected from the lowermost and uppermost parts of the Kharus Formation in Wadi Bani Awf, utilizing U-Pb radiometric methods. The obtained ages were 573 ±28 and 564 ±4.5 Ma, respectively (error margin, i.e., sigma 1 or 2 not provided). Based on U–Pb zircon ages from volcaniclastic rocks of the overlying Fara Formation, Bowring et al. (2007) interpreted the age of the top of Kharus Formation to be >547–544 Ma. Cozzi et al. (2004) constrained an age for the top of Buah Formation (the equivalent of Kharus Formation in the Huqf area) of 550 Ma, based on global chemo-stratigraphic correlations and the sediment accumulation, dating the deposition of Buah Formation as a whole between ca. 555 Ma and 550 Ma.

The 380-m-thick Fara Formation, exposed in Wadi Bani Awf, has been divided in three members in other studies (Beurrier et al., 1986; Béchennec et al., 1992). The lower member consists of 60-m-thick black cherts interbedded with grey dolostones (Béchennec et al., 1992), the top part containing meter-thick layers of banded silicic tuff (Béchennec et al., 1992). The 200-m-thick middle member is characterized by conglomerates, siltstones, breccias, grit, sandstones, sandy limestones, stromatolites, and abundant phosphate grains (Beurrier et al., 1986). The 120-m-thick upper member is also lithologically diverse consisting of quartzose siltstones, grey-green argillaceous siltstones, green silicic tuffites, greywackes, sandstones, and carbonate-cemented conglomerates (Béchennec et al., 1992). Based on stratigraphic observations, Al Rawahi et al. 92018) proposed subdividing Fara Formation in five members.

The change from the stromatolite-bearing limestone deposits of the Kharus Formation to the silica-rich sedimentary deposits (or silicilyte of Al-Rawahi et al., 2018; see also Amthor et al., 2005; Stolper et al., 2017) of Fara Formation reflects a basin deepening (Allen, 2007; Bowring et al., 2007).

The Fara Formation is considered by previous authors as a partly time-equivalent sedimentary sequence to the Ara Group (e.g., Forbes et al., 2010). Brasier et al. (2000) described an ignimbrite level within Fara Formation, 200 m above the base of the formation, which yielded 544.5 ±3.3 Ma U–Pb zircon ages. Bowring et al. (2007) determined two additional U–Pb zircon ages from volcanic rocks of the Fara Formation. The weighted mean ages of 547.23 ±0.28 and 542.54 ±0.45 Ma are from the base and top of the formation, respectively.

The above descriptions of the Kharus and Fara formations and the subdivision of Fara into members derived from studies in Wadi Bani Awf (Beurrier et al., 1986; Béchennec et al., 1992), but a recent road cut has offered superbly exposed new outcrops, allowing the additional detailed stratigraphic observations developed in this study.

The Ara Group from Interior Oman

U–Pb zircon dating of a tuffite from the subsurface of the lower and middle parts of the Ara Group, occurring in the South Oman Salt Basin, revealed ages of 546.72 ±0.21 Ma, 548.9 ±0.98 Ma (Bowring et al., 2007) and 542.6 ±0.3 (Amthor et al., 2003), respectively. The overall age of the Ara Group is ~547–538 Ma (Forbes et al., 2010). In contrast to Fara Formation, the southern Ara Group consists of six cyclic evaporite-carbonate sequences with shales, embodying a high potential for hydrocarbon seals (e.g., Mattes and Conway Morris, 1990; Amthor et al., 2003; Schröder et al., 2003; Forbes et al., 2010). Evaporites of the Ghaba Salt Basin may extend north of the thrust front of the Hawasina nappes below the south-eastern Oman Mountains, but still south of the Saih Hatat Dome (Mount et al., 1998; Heward and Penney, 2014). No sedimentary rocks of the Ara Group have been mapped or reported so far from the latter dome.

METHODS

This work is based on the detailed bed-by-bed description of five logs of Fara Formation in Wadi Bani Awf, with a cumulative thickness of 415m. The respective lithostratigraphic columns are provided in the Appendix section (logs 1-5, appendices 1 and 2). Structural measurements were carried out, providing dip direction, dip angle, trend, and plunge data. To better define the tectonostratigraphic evolution of Fara Formation, eight samples (FA1, FA2, FA4, FA5a, FA5b, FA6, NF1 and NF2 - Appendix 1 for the stratigraphic positions) were collected, each representing a different stratum of volcaniclastic lithologies within Fara Formation, for major- and trace-element determinations, performed at Activation Laboratories Ltd. (Ancaster, Ontario, Canada). The major elements were measured using an ICP-OES (0.2 g of sample pulp by lithium metaborate/tetraborate fusion), yielding detection limits in the 0.001-0.01% range. Trace element compositions were determined with an ICP-MS, following dilution of fused samples in 5% HNO_3. The analysed sample sequence included calibration and verification standards, alongside reagent blanks. Reported trace element detection limits fall in the 0.01-0.5 ppm range.

FIELD RESULTS

Lithostratigraphy and interpretations of depositional environments

Bed-by-bed analyses and descriptions were carried out from the top the Kharus Formation (23°16 '45" N - 57°27'47" E; see the coordinates of starting point in Appendix 1 and for the locations see Appendix 2). The top of the Kharus Formation is characterized by massive dark fetid grey dolostones with centimetric phosphate nodules (Fig. 3a and 3b), firstly described by Beurrier et al. (1986). A disconformity marks the contact with the overlying Fara Formation (Fig. 3a), due to an erosional/non-depositional interval at the boundary between the two formations. The bottom of the latter begins with an alternation of decimetric to sub-metric, well-bedded, laminated, dark coloured dolostones with centimetric grey and brownish siltstones, fine-grained sandstones, and thin layers of light grey laminated volcanic ash material, weakly laminated dolomitic limestones and boudinage dolomite beds. The beds generally dip towards the N with a dip angle of 40°.

Figure 3. (a) – Contact between the Kharus and Fara formations (FA1 member). (b) – (FA1) Well-bedded grey dolostones in the wadi with phosphate nodules (black round objects, diameter 1-3 cm). (c) - (FA1) Slumped debritic/mud-flow deposit (dashed blue lines). (d) - (FA1) Details of a slump level. (e) - (FA1) 2-m-thick slump level.

Six meters above the base of the formation, a slumped debrite/mud-flow deposit occurs (Fig. 3c blue dashed line), comprising grey volcanic ash, dolostone lenses, laminated dolomitic limestones and rusty fine-grained clastic sedimentary rocks (Fig. 3d and 3e). Verging slump folds indicate a transportation to the N/NNW. The early diagenetic structures indicate some gravitational slope instability, possibly caused by uplift to the S/SSE. Further slope instability is documented in the lower and middle members of Fara Formation (FA1, FA2). This is followed by an alternation of grey dolomitic limestones, fine-grained sandstones with crossbedding, a debritic level with dolostone clasts and some centimetric grey mudstone beds. After some non-exposure of $\sim$10 m, the lithostratigraphy of Fara Formation is represented by $\sim$90 m of laminated, dark, rusty, and finely laminated silicilyte, containing <2-m-thick dark brown dolomitic boudins (Fig. 4a).

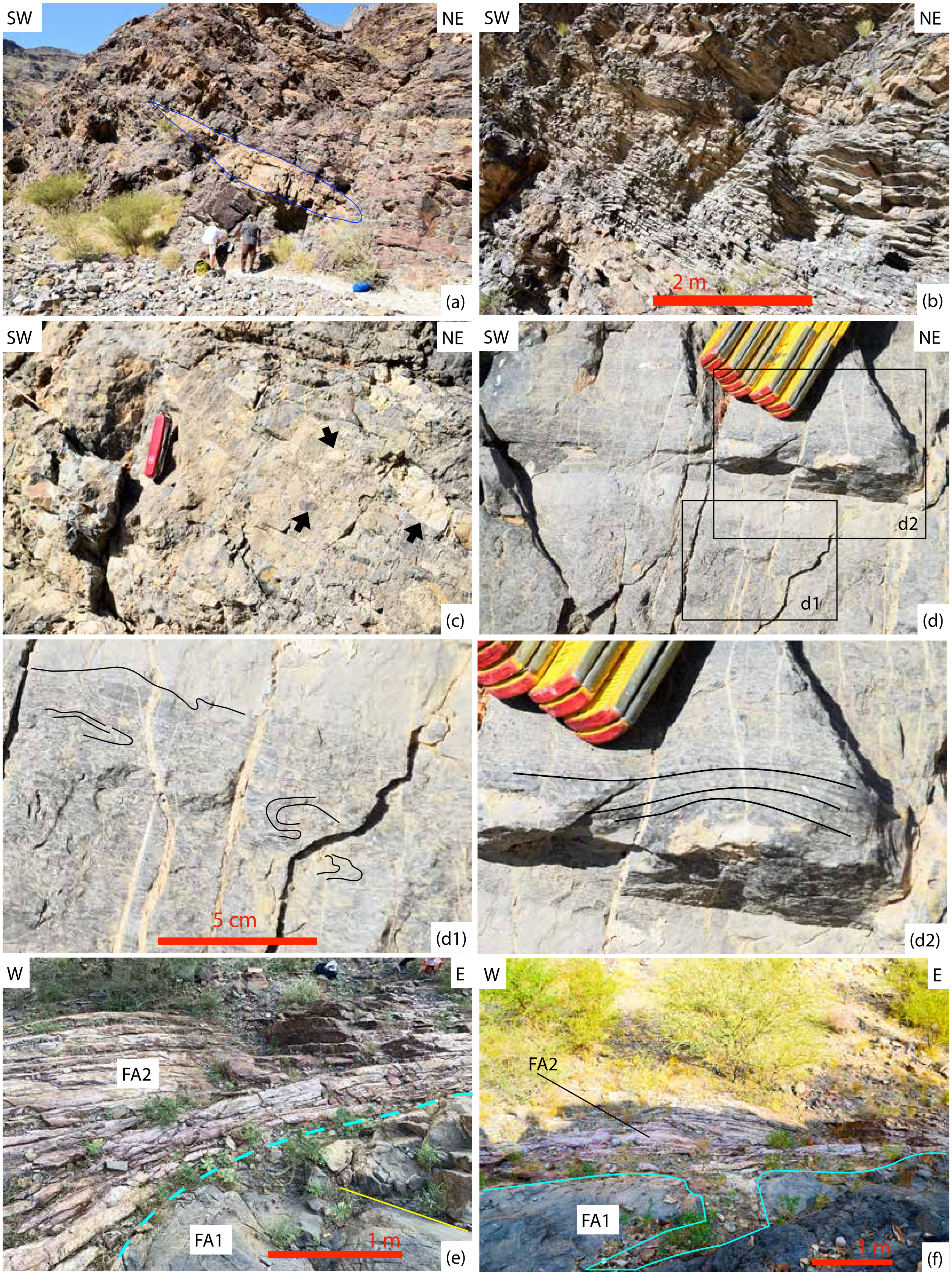
SW
NE
(a)
SW
NE
2 m
(b)
SW
NE
(c)
SW
NE
d2
d1
(d)
5 cm
(d1)
(d2)
W
E
FA2
FA1
1 m
(e)
W
E
FA2
FA1
1 m
(f)

245

Figure 4. (a) – (FA1) Thick-bedded dark grey silicilyte with a brown dolomite boudin (blue line). (b) – (FA1) Thick- to thin-bedded (from left to right) dark grey silicilyte. (c) - (FA1) Grey sedimentary breccia with clasts of grey and white dolomite. (d) - (FA1) Dark grey stromatolitic dolostone, (d1) detail irregular and folded stromatolitic structures, (d2) detail of a stromatolitic structure. (e) and (f) - contact between FA1 and FA2. Contact is marked by an onlap of fine-grained deposits onto the underlying stromatolitic dolostone in (e), and by a filled fracture within the dolostones in (f).

The thickness of the silicilyte layers decreases towards the top, from decimetric to a few centimetres (Fig. 4b, bedding 350/45). This unit is characterized in the middle/upper part by a 2-m-thick slump with a transport direction to the ESE, followed by an alternation of silicilyte with very thin-bedded claystone. After 10 m of thin- to medium-bedded silicilyte with dolomitic boudins, the lithology changes to a ~10 m thick sequence of laminated dark grey dolostones, followed by a 1-m-thick horizon of sedimentary breccia (Fig. 4c) with dolostone clasts (<15 cm in diameter). The upper part of the latter unit is characterized by fetid, very-thin laminated stromatolitic dark grey dolostones with typical low domal and irregular stromatolitic structures (Fig. 4d1 and 4d2). Towards the W (50 m along the strike direction N50; Appendix 2), dark grey, well-laminated fetid stromatolite-bearing dolostones are exposed with pockets and dikes of volcaniclastic/volcanic rocks (Fig. 4e and 4f). The dolostones appear disassembled in blocks, separated by fractures filled with pinkish-ochraceous fine-grained deposits, testifying fracture opening during sedimentation in response to the onset of brittle deformation (Figs. 4e, 4f and 5a).

Figure 5. (a) - Contact between dark grey stromatolitic dolostone with a quartz-filled fracture (FA1) and overlying light grey to pinkish fine-grained volcaniclastic sediments (FA2). (b) - Detail of a coarse-grained neptunian sandstone dike, cutting thin-bedded cherty siltstone (FA2). (c) - Detail of a folded Neptunian dike (FA2). (d) - Fold-and-thrust structure in thin-bedded cherts (FA2). (e) - Asymmetric boudins of conglomerates

and sandstone with D2 thrusts, testifying shortening (FA2). (f) - Details of the terminal portion of a grey sandstone boudin (FA2). (g) - Details of a conglomerate, consisting of grey dolostone clasts (FA2). (h) – Current markers at the base of a grey sandstone, denoting a NW-directed paleocurrent (FA2).

In the present study, the top of the stromatolitic dolostones is considered as the top of the ~130-m-thick FA1 member. Overall, at the base FA1 consists of shallow-marine carbonates, marking the transition from the shallow-marine Kharus Formation. The stromatolites further up indicate a shallow-marine depositional environment as well. The silicilyte formed under more basinal conditions, with reduced siliciclastic input, as part of a transgressive to high stand system tract, and in a reducing, probably anoxic environment (Amthor et al., 2005). FA1 displays gravitational slope sedimentary features (slumps, sedimentary breccias). The very top of FA1 is characterized, again, by shallow-marine carbonates.

The pinkish, fine-grained volcaniclastic rocks overlying the stromatolites are considered as the base of FA2 (Fara Formation member). In general, the basal volcaniclastic rocks, followed by a clastic succession, characterize FA2, starting with 20 m of thin- to thick-bedded alternations of light grey to pink thin-bedded chert, siltstones, and sandstones with carbonate grains and carbonate matrix. In places, such grading is reversed. This alternation contains Neptunian dikes (Fig. 5b) consisting of coarse-grained sandstones, probably formed during slumping (Fig. 5c). Further up in the sequence, FA2 is reveals a 22-m-thick alternation of fine-grained and medium- to thick-bedded rusty sandstones, displaying metric folds and thrusts (Fig. 5d). The following succession is laterally discontinuous, with lenticular rock units. To the west, a 5-m-long lens of a polymictic, poorly sorted conglomerate with sandstone matrix is exposed. Towards the east, the abundance of conglomerate lenses gradually increases, but assuming smaller sizes, giving rise to symmetric and asymmetric boudins, which indicate a tectonic transportation towards the SE, (Fig. 5e-g). This unit is topped by a 30-m-thick succession of brownish and thin- to medium-bedded sandstones with carbonate matrix. Basal NW/SW-trending non-polar paleocurrent indicators are common (Fig. 5h), caused by suspension currents. This succession ends with a metrically thick layer of oligomictic conglomerates/breccias of black fetid limestone and light grey dolostone clasts. The top FA2 consists of a tuffite of variable thickness, followed by a ~50-m-thick alternation of grey sandstones and fine-grained sandstones with carbonate matrix (Fig. 6a).

Figure 6. (a) -Alternation of grey sandstone and fine-grained sandstone (FA2). (b) – Load casts at the base of a 2-m-thick sandstone bed (FA2). (c) and (d) - Lower part of FA3, characterized by a 2-m-thick very fine-grained well-bedded and thinly bedded volcanic ash. (e) - Alternation of thick-bedded fine-grained sandstones and thin-

bedded siltstones (FA3). (f) - Detail of 1-m-thick graded tempestite bed (FA3). (g) - Grey sandstone with prod marks, indicating SE-directed suspension current transport (FA3).

This homogeneous succession ends with a single 2-m-thick bed of grey sandstones displaying load casts (Fig. 6b) beneath 2 m of grey, very fine-grained volcanic ash (Fig. 6c and 6d). The sandstone bed represents the top of FA2, which has a thickness of ~175 m, while the ash layer marks the base of FA3 (Fara Formation member 3).

Overall, FA2 consist of mostly siliciclastic and volcaniclastic rocks. The breccias and slump folds indicate considerable tectonic uplift of FA2 during deposition accompanied by subsequent volcanic activity. The paleocurrent marks indicate that the paleo slope was dipping towards the NW. Suspension deposits (tempestite and/or turbidites) and the absence of stromatolites could indicate a deeper depositional environment compared to FA1´s.

FA3 starts with an alternation of grey thin- to medium-bedded, fine-grained sandstones with thin-bedded siltstones (Fig. 6e), followed by a 1.2-m-thick tempestite (turbidite?) (Fig. 6f) and 5 m of bedded grey siltstones. This sequence is followed by a 12-m-thick alternation of grey, thin- to medium-bedded, fine-grained sandstones and thin-bedded siltstones with carbonate cement. Overlying the latter, decimetric grey sandstones with vortex-type wave-ripples (Figs. 6g, 7a) and flame structures are covered by 12 m of poorly bedded grey sandstones, followed by 1 m of grey siltstones, an alternation of thin- to medium-bedded, fine-grained sandstones and thin-bedded siltstones, and 1 m of a light grey volcaniclastic ash horizon (Fig. 7b and 7c).

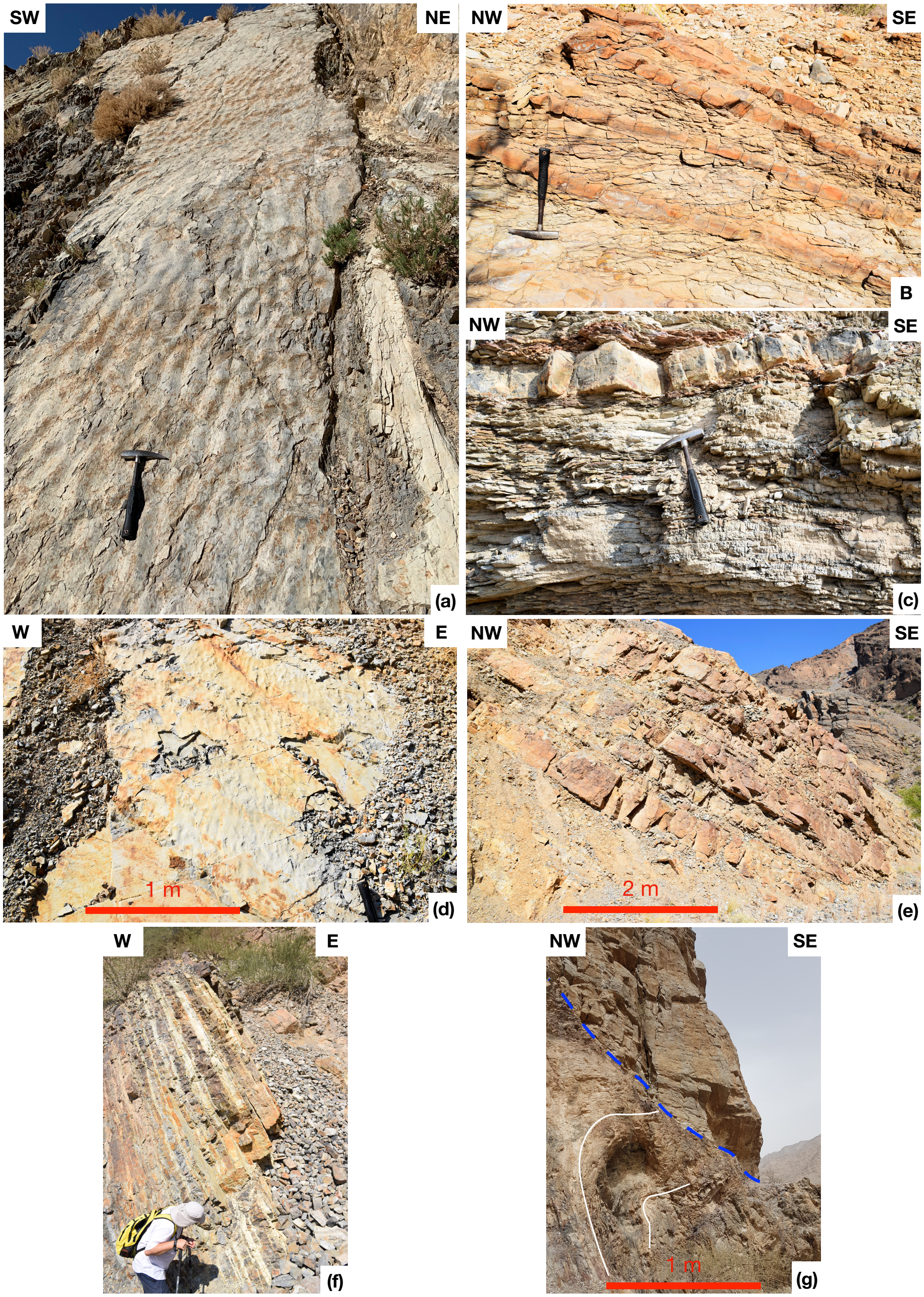

Figure 7. (a) - Grey sandstone with symmetric, wave-formed, vortex ripples (FA3). (b) - Alternation of medium- and fine-grained sandstones with light grey thin-bedded siltstones (FA3). (c) – One-m-thick light grey volcaniclastic bed (FA2). (d) - Fine-grained rippled sandstones with paleocurrent direction W-E (FA3). (e) and

(f) - Upper part of FA3, characterized by an alternation of light grey siltstones with grey sandstones. (g) - Angular unconformity between folded FA2 and the overlying Permian rocks.

Fine-grained rippled sandstones top the ash bed (Fig. 7d), displaying current ripples, indicating a focal paleocurrent direction towards N98. An alternation of grey siltstones and medium-bedded sandstones follows this succession (Fig. 7e and 7f). Towards the top of the siltstone/sandstone alternation, a single *Palaeopascichnus* specimen was discovered (see below). The succession is followed by a 5-m-thick alternation of grey volcaniclastic, fine- to medium-grained sandstone, 4-m-thick fault breccia and 10 m of light grey, medium-bedded, fine-grained sandstones. Furthermore, a 12-m-thick section of poorly bedded, cross-bedded, fining-upwards laminated grey sandstones, with basal scours in some layers, occurs, ending with a grey, medium to thick-bedded sandstone. FA3, with a total thickness of ~107 m, ends with 20 m of a monotonous sequence of fine- to medium-bedded, fine-grained sandstone beds, with some levels of well laminated grey siltstones.

The total thickness of Fara Formation amounts to ~412 m, which represents the minimum thickness because the top parts of the formation are truncated below an ungular unconformity (Figs. 7g, 8a and 8b). The overlying Permian Saiq Formation consists of a few-meters-thick basal conglomerate (Fig. 8c) and coarse-grained sandstones (1-2 m in thickness) followed by bluish grey bioclastic dolostones and limestones. The clastic components of the basal conglomerate are well-rounded, exhibiting grain support. Considering the erosional gap at the angular unconformity as well as both the clast rounding and support fabric, we interpret the basal conglomerate as a transgression/beach conglomerate.

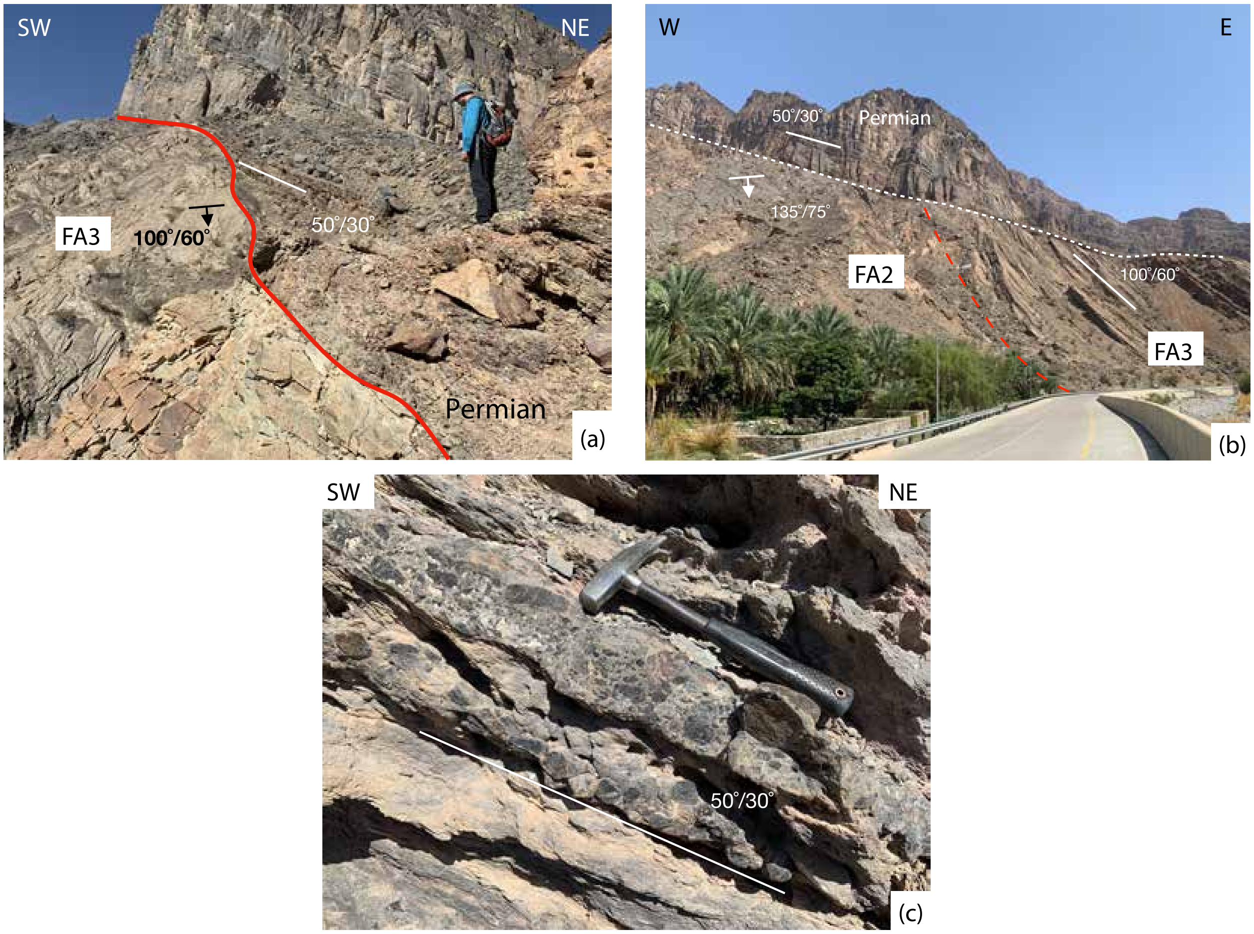

Figure 8. (a) – Unconformity between FA3 and the Permian Saiq Formation. Note the basal conglomerate of the Saiq Formation. (b) – Panoramic photograph of the "Hercynian" unconformity (white dashed line) and the Cadomian angular unconformity (red dashed line), dipping towards the NE. NE tilting of the unconformity relates to Cenozoic doming of the Jabal Akhdar. (c) – Basal conglomerate of the Saiq Formation.

Palaeontology – *Palaeopascichnus linearis*

A carbonate body fossil of 7 cm length (Fig. 9) was discovered in the upper part of FA3 member (see above and Appendix 1 for location). Grading within the host rock suggests that this lifeform was fossilized at the base of a siltstone/fine-grained sandstone bed. The elongate fossil is characterized by a uniserial arrangement of oriented saucer-shaped discoidal structural elements (Fig. 9a), each single disc measuring <1 cm in diameter. The concave sides of the discoidal segments are systematically facing the same direction (Fig. 9a and 9b). Moreover, the arrangement is displaying the onset of segment bifurcation (right side of Fig. 9a). We consider the fossil as a rare example of *Palaeopascichnus jiumenensis* (Fig. 9b) or *Palaeopascichnus linearis*, based on the morphological comparison (Dong et al. 2008; Kolesnikov et al. 2018). Based on morphological features, Dong et al. (2008) argue that *Palaeopascichnus* may be phylogenetically related to agglutinated foraminifers. This fossil, discovered in FA3, represents the first known occurrence of a macroscopic Ediacaran body fossil at the surface of Oman, therefore assigning an Ediacaran age to the top of Fara Formation. Wells targeting the subsurface Ara Group (A1-A3 carbonate unit) in Interior Oman report the presence of *Cloudina* and *Namacalathus* (Amthor et al., 2003).

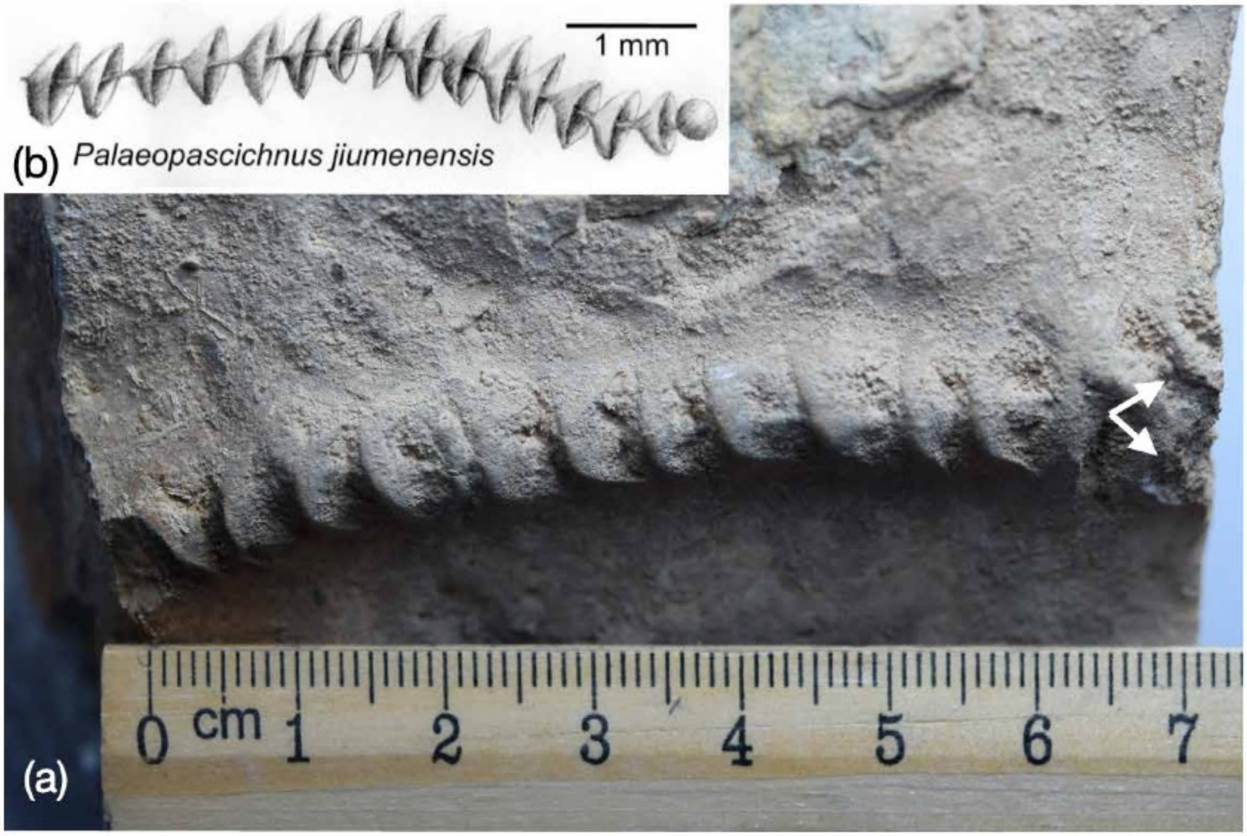

Figure 9. (a) – Fossil discovered in FA3 at the base of a siltstone/fine-grained sandstone bed. The fossil itself corresponds to a carbonate filling, displaying the onset of segment bifurcation on the right-hand extremity (white arrows). GPS coordinates of locality: 23°17'14" N - 57°27'59" E. (b), Palaeopascichnus jiumenensis as described by Dong et al. (2008).

.

Structural geology

Field studies demonstrated that a low-angle angular unconformity occurs between FA2 and FA3 members. The bedding planes at the top of FA2 dip 110/74, while at the base the bedding attitude of FA3 is 090/70. The orientation of the angular unconformity is 090/65. Fara Formation´s members FA1 and FA2 display a variable bedding orientation and two sets of cleavage (Figs. 10 and 12; S1 and S2).

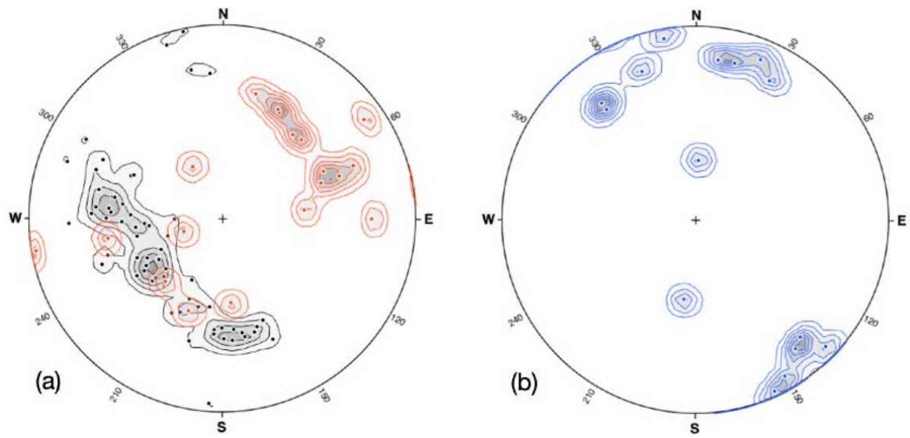

Figure 10. Lower hemisphere stereographic equal-area projection of S0. Measurements taken from FA2 and FA3. (a) stereoplot - 83 poles of S0 (red), 19 poles of S1 (black). (b) stereoplot - 15 poles of S2 (blue).

S1 orientation is variable but dips in general moderately to the NE. S2 is mostly steeply dipping and strikes NE/SW.

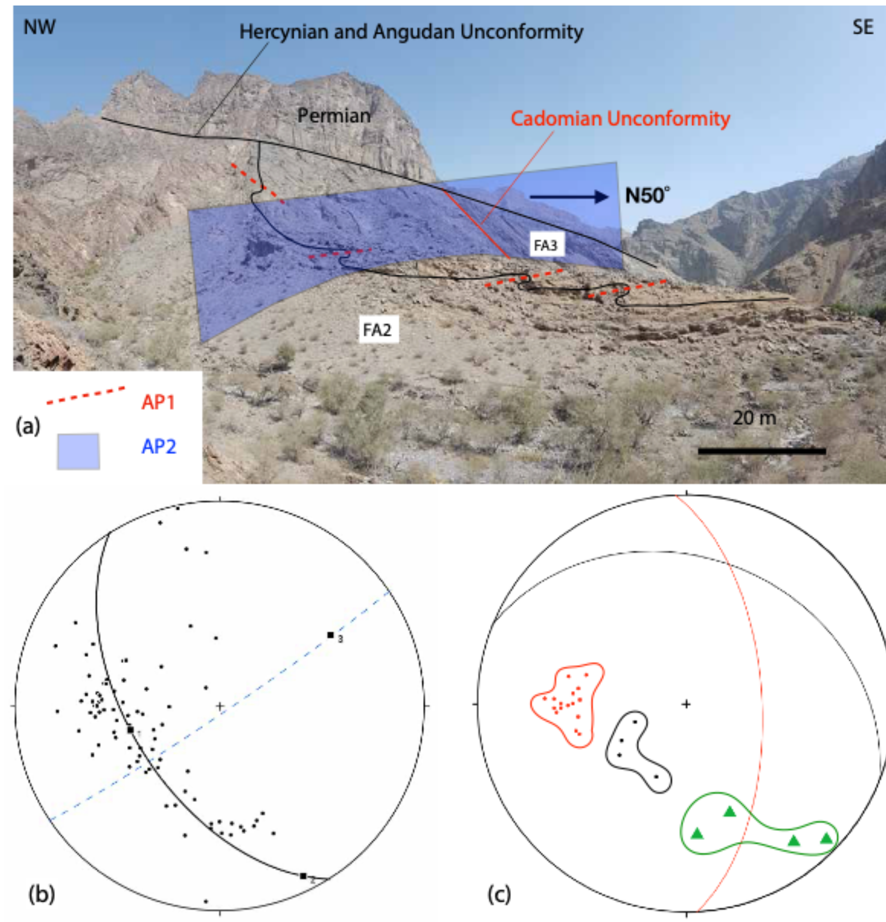

Figure 11. (a) - The black folded line highlights the overall structural style of S0 inside FA2 (not a geological boundary), showing the effect of D1 deformation (Cadomian event in Callegari et al., 2020). D1 developed AP1 axial planes with fold axes trending N135. These folds are refolded by D2 event (Angudan event). (b) Lower hemisphere stereographic equal-area projection of 83 poles of S0, on point 3 the trend and plunge of D2 fold axis: 057-36, dashed blue line is the D2 axial plane: 147/89. (c) Lower hemisphere stereographic equal-area projection of 24 poles of S0 The S0 poles from FA1 and FA2, FA3 and the Permian are marked in green, red, and black, respectively. The red great circle represents the focal orientation of the Cadomian Unconformity (090/65). The black great circle depicts the "Hercynian Unconformity" and the Angudan Unconformity.

Furthermore, FA1 and FA2 members contain tight cylindrical folds (hereafter F1) with an amplitude of a few meters. The trend of these folds axes changes from N135 in the north-western sector to N045 in the south-eastern sector (Figs. 13 and 14), a variation is attributed to refolding (Fig. 10 left).

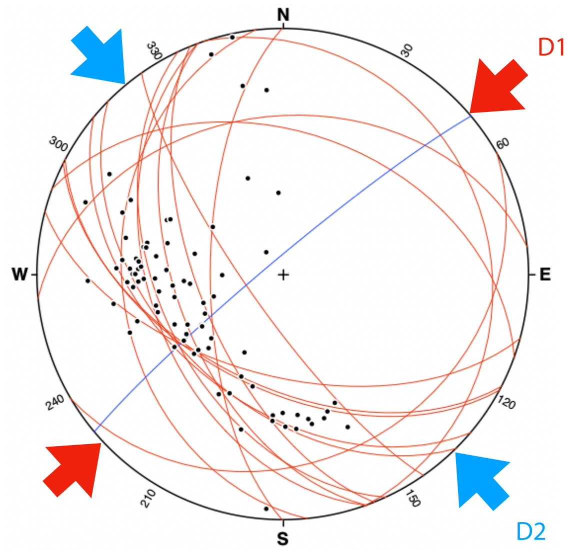

Figure 12. Lower hemisphere stereographic equal-area projection of 83 poles of S0. Red great circles represent 19 S1 measurements, and the blue line is the axial plane of the D2 open fold. Shortening directions during D1 (Cadomian) and D2 (Angudan) events. FA1 and FA2 record D1 and D2 structures, while FA3 records D2 structures, only.

The dominant S2 cleavage strikes N50-N70, with variable dip angles, but mostly steep (Fig. 10 right).

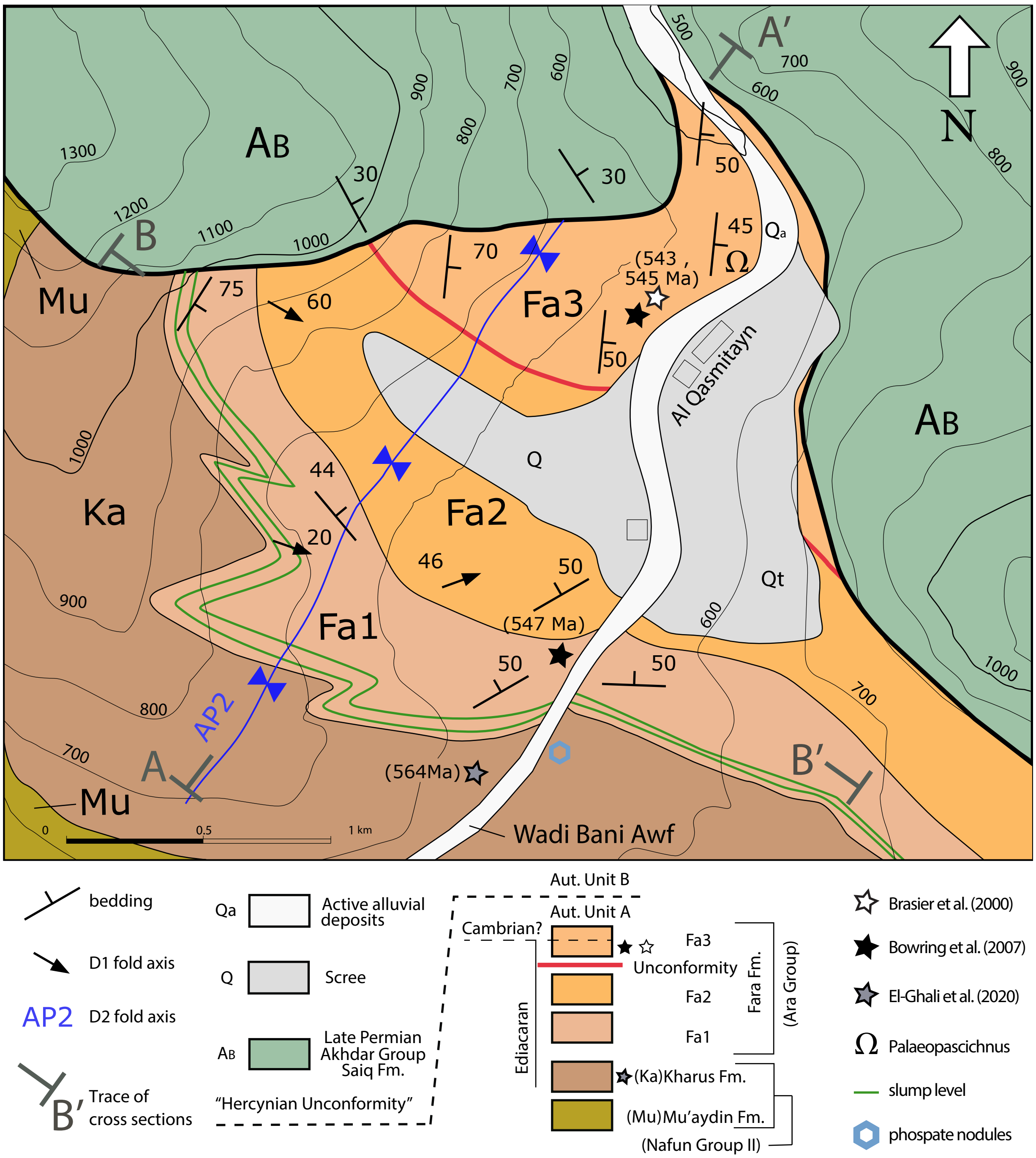

Figure 13. Geological map of Fara Formation and its surroundings in Wadi Bani Awf. Equidistance of contour lines is 100 m.

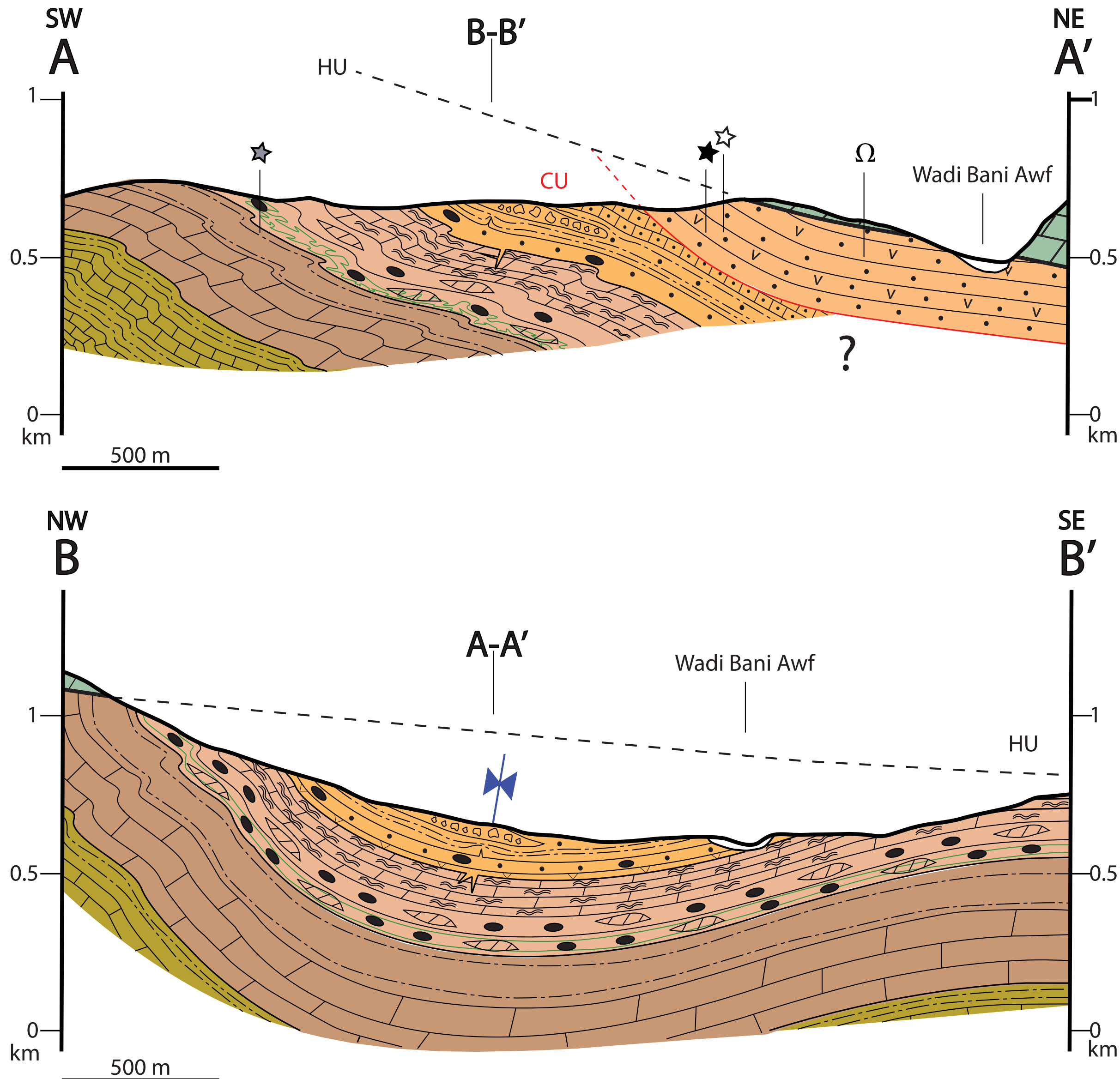

Figure 14. Geological cross sections of the Fara Formation in Wadi Bani Awf. Note that F1 folds are only observed in FA1 and FA2 but not in FA3. HU - "Hercynian Unconformity". For the legend see Appendix 4.

The F1 fold axial planes dip shallowly to the NW in the southern part of the study area (AP1 in Fig. 11), and to the SE close to the "Hercynian Unconformity" in the northern sector (Fig. 11), and were refolded by an open F2 syncline, with an amplitude of some hundred meters (Fig. 11). The axial plane of the F2 fold (AP2 in Fig. 11) is oriented 140/85.

In FA1 and FA2 members, we recognized and confirmed two pre-Permian deformation events (compare Callegari et al., 2020; Scharf et al., 2021a). As demonstrated by Callegari et al. (2020) and Scharf et al. (2021a), who studied the western-central Jabal Akhdar Dome, the interpretation of the pre-Permian folds and structures reveals a superimposed fold structure. F1 folds are well exposed in FA2 due to the overall shaly lithology. F1 hinges are often truncated by ductile shear zones and thrusts. The orientation of D1 structures indicates that the maximum shortening direction related to D1/F1 was ~NE/SW-directed, with the fold vergence towards the NE. D1 structures were refolded by D2 structures.

The F2 syncline differs in style and orientation from the F1 folds. The F2 fold axial plane is sub-vertical and strikes NE-SW, indicating a sub-horizontally NW/SE-oriented shortening direction (D2 event in Fig. 12). The F2 fold axis plunges ~55–60° to the NE (left side in Fig. 11). Moreover, the superimposed fold structure in the study area has been rotated ~30° along a WNW/ENE-trending horizontal rotation axis, during the Cenozoic D3 doming (Scharf et al., 2021a).

D1/F1 structures can be observed in FA1 and FA2 members, but not in FA3. Furthermore, the base of FA3 is marked by an angular unconformity. This demonstrates that the D1/F1 event predates FA3 deposition, i.e., D1/F1 is of latest Ediacaran age.

The entire Fara Formation has been affected by the D2/F2 open syncline. This syncline, with a wavelength of hundred meters, displays a steeply dipping north-western limb and a moderately, steeply dipping south-eastern limb (Figs. 13, 14).

Petrography of volcaniclastic rocks

We collected eight samples of volcaniclastic rocks belonging to Fara Formation. Two samples (NF1, NF2) where collected from the bottom of FA2 member, while the remaining six are from the lower part of FA3 member (see Appendix 1 for sample locations).

Samples NF1 and NF2

The two samples of volcaniclastic lithologies from FA1 member both display fine-grained textures (siltstone). Their mineralogy is dominated by sub-angular to angular quartz grains in a matrix of sericitized plagioclase/alkaline feldspar, with minor amounts of chlorite and interstitial opaque microliths. Among the latter, leucoxene and rutile are the predominant phases. These rocks are crosscut by microscopic veins with varied mineral contents, such as secondary quartz, carbonates, barite, and reddish opaques (Fe and Ti oxides). At instances, both carbonate and barite veins reveal mineralogical zonation, with opaques occurring along the walls of microfractures, and carbonates/barite occupying the central areas. The observed secondary mineral paragenetic associations indicate that the primary assemblages were subjected to hydrothermal alteration in a multistage process, which included sericitization, chloritization, silicification, and carbonatization underpinned by a change in fluid redox conditions towards a more oxidizing media.

Samples from FA1 to FA6

A detailed petrographic analysis of the volcaniclastic lithologies from the FA3 member is included in Pinto et al. (2020), and the same strata have been re-sampled for the present study. Similarly, to FA2 member volcanic rocks, these lithologies are characterized by fine-grained textures but reveal notable variations concerning mineral contents. In comparison to samples NF1 and NF2, FA3 lithologies show a less conspicuous prevalence of quartz, higher contents of sericitized plagioclase/alkaline feldspar, and contain shards of devitrified glass (Fig. 15a and 15b).

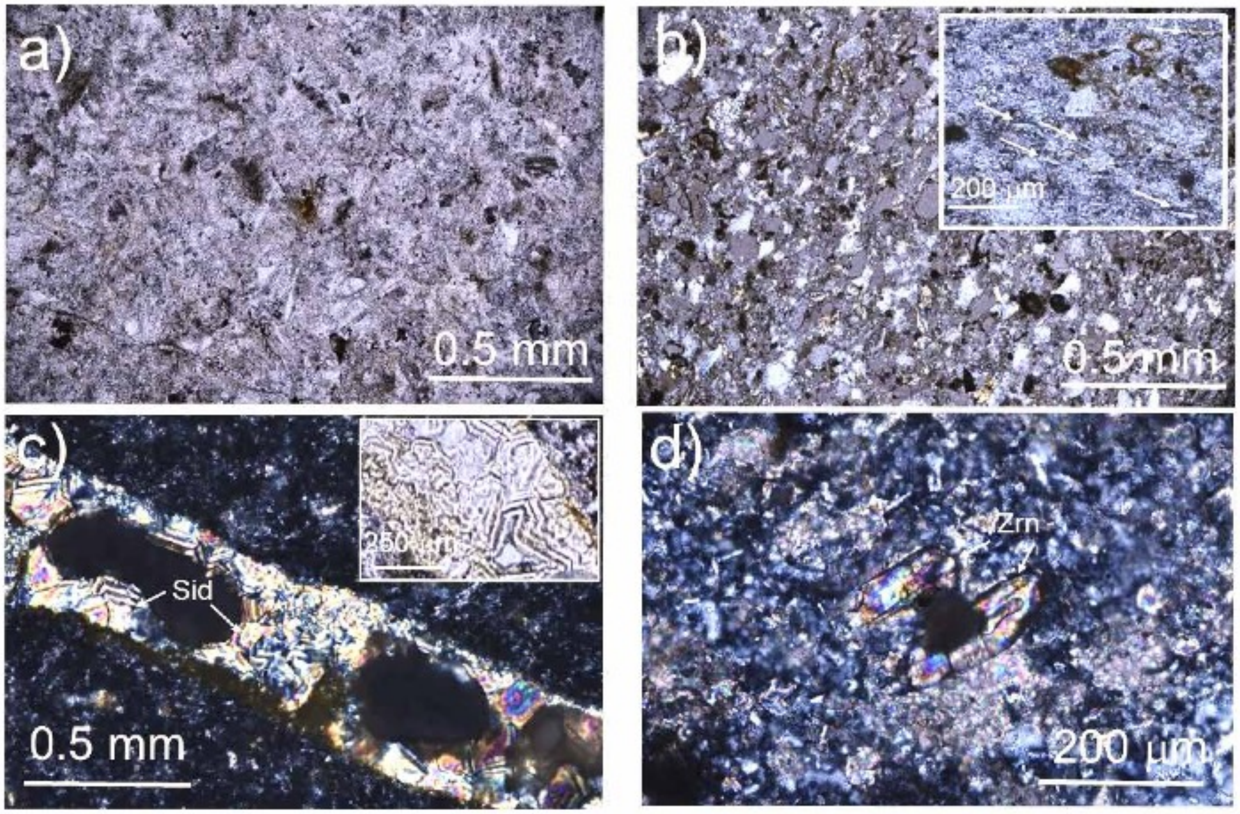

Figure 15. Optical micrographs of lithologies from FA3: (a) glass shard and zircon bearing ash tuff (plane-polarized light), (b) quartz-rich ash tuff (crossed-polarizers), with an oriented fabric of phyllosilicates (inset, plane-polarized light), (c) vein of siderite in an ash tuff (crossed nicols), displaying zoning and intergrown $\{011\bar{2}\}$ twins (inset, plane-polarized light), (d) zircon individuals in lithic ash tuff, embedded in a saussuritized matrix. Sid = siderite, Zrn = zircon.

A particular dark-coloured bed corresponding to a zircon-bearing lithology was the subject of previous geochronological investigations (Bowring et al., 2005; Brasier et al., 2000), with the purpose of determining the absolute age of this formation. The different FA3 volcaniclastic rock occurrences reveal heterogeneous hydrothermal alteration features, both in terms of mineral products and extent of replacement of the original assemblage, with some lithologies displaying a nearly complete obliteration of primary phases by hydrothermal reaction products. FA3 samples display evidence of silicification, saussuritization, sericitization, epidotization, chloritization and carbonation, with different degrees of alteration intensity. The inset of Figure 15b is a plane polarized-light micrograph illustrating the preferential orientation of phyllosilicates (sericite and chlorite) in these lithologies. Given the clastic nature of these rocks, it is very unlikely that the incipient fabric is an inherited feature and should instead reflect a response to a stress field. The opaque grains, present in all lithologies, correspond to associations of goethite, TiO_2 phases, and leucoxene. FA3 lithologies seem to become more “ignimbritic” upwards in the stratigraphic succession, with glass shards included in the clastic fraction, alongside quartz-filled amygdules. Regardless of the involved volcanic phenomena and associated variations in transport mechanisms, the observed grainsizes allow to classify these rocks as "tuffs". In the current study, during both field and petrographic investigations, we did not find any welding or black flame features as described by McCarron (1999) and mentioned by Bowring et al. (2007). The extensive hydrothermal alteration frequently obscures both primary mineralogy and textural features of the protolith, except for relicts and pseudomorphic replacements. Sericitization, silicification, and carbonatization alteration products can mostly be found in the matrix of these rocks, while fine-grained saussuritization assemblages replace glass shards and plagioclase. The occurrence of carbonate and quartz veins crosscutting these rocks is another testimony of intense hydrothermal activity having affected these rocks. Quartz veins commonly display ondulose extinction, while siderite veins have also been observed (Fig. 15c). Siderite occurs in open druses, as euhedral intergrown and zoned individuals, commonly displaying the $\{01\bar{1}2\}$ twin law, increasing in coarseness and becoming progressively idiomorphic from the fracture walls inwards, following a typical geometrically selective growth pattern. In lithologies rich in glass shards, such as exemplified by figure15a, zircon crystals with maximum lengths of <200 μm are found dispersed throughout the clastic fraction of the rock. Figure 15d depicts two zircon individuals under crossed nicols, embedded in a saussuritized matrix. In the observed zircons, the common combination of the tetragonal prismatic and (bi)pyramidal forms is discernible, though frequently the sections' outlines are not fully idiomorphic, revealing curved edges. Furthermore, zircon individuals are seldom devoid of cracks, especially transversal to the crystals' lengths.

Whole Rock Geochemistry

As evident from the thin-section analyses, considerable hydrothermal alteration affected all sampled lithologies, precluding the use of major element classification schemes, especially those based on alkali elemental contents. Nevertheless, the six analysed samples of FA3 yield values of 64.23 < wt.%SiO_2 < 78.04, 0.75 < wt.% K_2O < 6.46 and 0.41 < wt.% Na_2O < 6.11 (Appendix 3 for complete analytical results). In agreement with the petrographic observations and compared to the results obtained for FA3 volcaniclastic rocks, the two samples of FA2 member volcaniclastic rocks contain higher levels of SiO_2 (~85-90 wt.%), and lower contents of both K_2O (~0.7-0.8 wt.%) and Na_2O (~0.05-0.12 wt.%).

Considering the limitations imposed by alteration on the use of whole rock geochemical tools, immobile elemental composition may offer alternative clues and insights for the geodynamical contextualization of the igneous materials. **Error! Reference source not found.**16a is a Th/Yb *vs.* Ta/Yb plot, as defined by Gorton and Schandl (2000), depicting data pertaining to both volcaniclastic lithologies of the Fara Formation (FA2 and FA3) and rhyolites from Hormuz Island (Faramarzi et al., 2015).

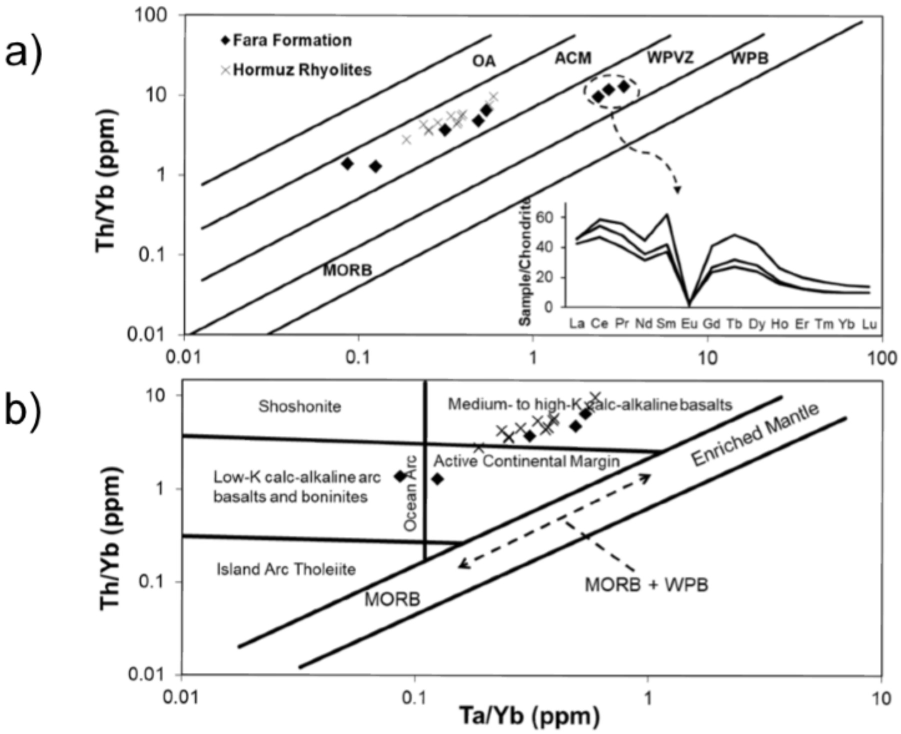

Figure 16. Th/Yb vs. Ta/Yb tectonic discriminant criteria according to (a) Gorton and Schandl (2000) and (b) Pearce (1983), displaying the compositional ratios of both FA2 and FA3 volcaniclastics and Hormuz Island rhyolites (Farmarzi et al., 2015). The included REE chondrite-normalized (McDonough and Sun, 1995) diagram in (a) is referent to highly altered samples, plotting within the compositional range of 'within plate volcanic zone' (WPVZ). OA=Ocean Arc, ACM=Active Continental Margin, WPVZ=Within Plate Volcanic Zone, WPB=Within Plate Basalts.

The latter yielded zircon ages of ~558 Ma (Faramarzi et al, 2015), near to the values of ~543 and 545 Ma determined by Bowring et al. (2007) and Brasier et al. (2000), respectively, which alongside the geographical proximity to the sampled locations, point towards the possibility of a shared tectogenetic setting. According to the criteria of Gorton and Schandl (2000), all samples but three reveal characteristics of igneous rocks formed at active continental margins (ACM), and plot together in the same field as representatives of rhyolites from Hormuz Island. The two data points in the ACM field with lower Th/Yb and Ta/Yb correspond to samples from FA2. A closer inspection of the three FA3 samples plotting inside the 'within plate volcanic zone' (WPVZ) reveals that these were affected by the highest intensity of hydrothermal alteration, especially sericitization. The inset in figure 16a shows the chondrite normalized REE (McDonough and Sun, 1995) compositions of these samples, providing clues on the degree of mobilization of trace elements by fluids. A striking feature of the displayed REE-normalized patterns is the large negative Eu anomaly coupled with a low LREE enrichment ($0.73 < La_{(n)}/Sm_{(n)} < 1.14$), a combination which cannot be attributed to magmatic evolutionary processes. Taking into consideration the high silica concentrations ($64.23 <$ wt.%$SiO_2 < 78.04$) in tandem with the defined mineralogical compositions of these samples, such REE characteristics point towards an important degree of trace element mobilization by fluids, and, therefore, they should be disregarded in the application of geochemical tectonic discriminant tools. The remaining dataset plots within the medium- to high-K calc-alkaline fields in the Pearce (1983) tectonic discriminant diagram, as displayed in figure 17b: the FA3 within the medium to high calc-alkaline basalts field together with the Hormuz Rhyolites, and the FA2 near the boundary between ocean arc and active continental margin compositions. The latter samples of volcaniclastic rocks include higher amounts of clastic quartz, which has a dilutive effect over whole rock trace element concentrations. Furthermore, these lithologies may include volcanic products erupted during an earlier and less alkaline stage of arc development.

Figure 17a documents the chondrite-normalized rare earth element (REE) patterns for the volcaniclastic lithologies of Fara Formation, together with those of three representative Hormuz Island rhyolites (Faramarzi et al., 2015). The applied normalization standard was the C1 chondrite REE composition from McDonough and Sun (1995). The obtained patterns display variable degrees of light REE (LREE) enrichment relative to heavy REE (HREE), as reflected by their wide range of overall slope values ($2.60 < La_{(n)}/Y_{(n)} < 8.16$). In the case of Fara Formation, the samples displaying both flatter patterns and lower levels of overall enrichment with respect to a chondrite standard are those belonging to the FA2, confirming the diluting effect of their high contents in quartz over trace element compositions. The HREE terminal section of all patterns is nearly flat, which alongside the strongly negative Eu anomalies point towards a shallow crustal magmatic source.

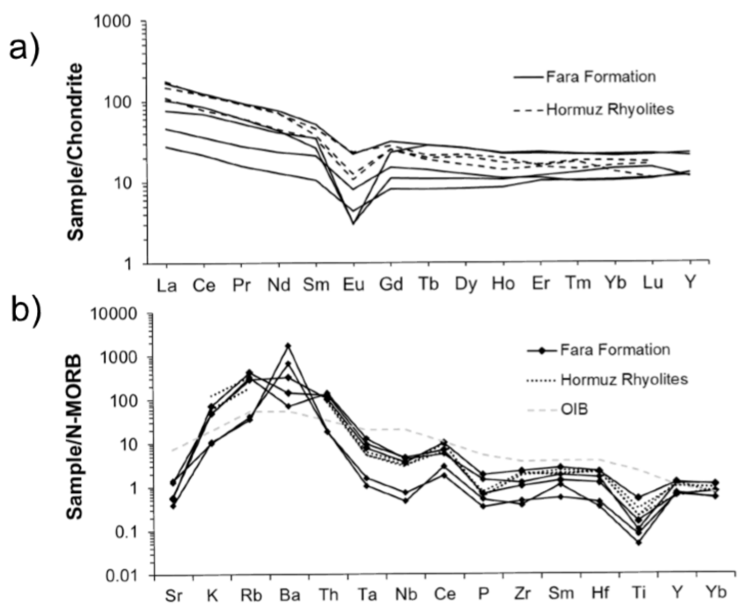

Figure 17. (a) - REE chondrite-normalized (McDonough and Sun, 1995) compositions of Fara Formation volcaniclastic rocks and Hormuz Island rhyolites (Faramarzi et al., 2015). (b) - MORB-normalized (Sun and McDonough, 1989) trace element compositions of Fara Formation and Hormuz Island rhyolites, using Pearce

(1983) trace element seriation. For comparison purposes, the normalized compositions of an average OIB (Sun and McDonough, 1989) are included.

Since the sampled lithologies correspond to crustal rocks, the mid-oceanic ridge basalt (MORB)-normalized, multi-elemental (Pearce, 1983) graphical depiction included in figure 17b is most suitable for gathering further petrogenetic insights. The normalizing N-MORB and normalized ocean-island basalt (OIB) values are from Sun and McDonald (1989). The patterns of both, Fara Formation volcaniclastics and Hormuz Island rhyolites display a remarkable degree of similarity, with a decoupling between high field strength (HFS) and large ion lithophile (LIL) elements, typical of subduction-zone magmatic products, together with Nb and Ti negative anomalies. The FA2 samples reveal lower degrees of enrichment relative to N-MORB, except for Ba related to the hydrothermal barite mineralization affecting these rocks. The values of Sr and Ba of the Hormuz rhyolites have not been reported by Faramarzi et al. (2015).

DISCUSSION

Age of Fara Formation

All volcaniclastic rock samples show evidence of hydrothermal alteration, which changed the whole rock geochemistry. Taking into consideration the type and extension of hydrothermal alteration affecting these lithologies together with all the described morphological issues in the zircon grains, it is worth considering the possibility that past geochronological determinations (Brasier et al., 2000; Bowring et al., 2007) have miscalculated the age of these lithologies, although both references report concordant values.

U-Pb zircon ages from Fara Formation yield 547 and 545-543 Ma from the lower and the top sections, respectively (Brasier et al., 2000; Bowring et al., 2007). Our petrographic and geochemical investigations targeting those same volcanic beds, demonstrates that significant hydrothermal alteration affects all lithologies. This suggests that the real age of these rocks could be older than the previously reported U-Pb geochronological determinations. Furthermore, the occurrence of the Ediacaran *Palaeopascichnus* organism in the FA3 member, stratigraphically above the dated volcaniclastics (Fig. 18) demonstrates that the entire exposed Fara Formation is Ediacaran in age (i.e., >538 Ma).

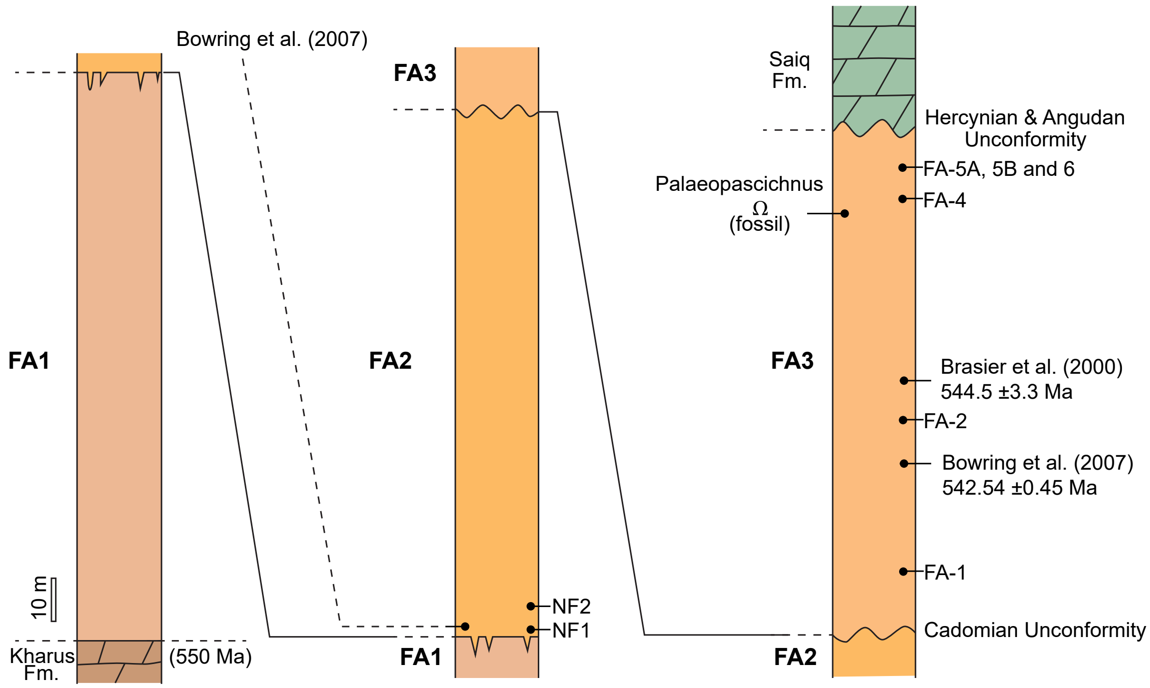

Figure 18. Schematic stratigraphic column of Fara Formation and sample positions. Legend in figure 13.

Ediacaran paleoenvironment and deformation

The sediments atop Kharus Formation are interpreted to have been deposited in a shallow-marine intertidal to supratidal environment (surface study by Béchennec et al., 1992) or on a distally steepened storm-dominated carbonate ramp (subsurface study by Cozzi et al., 2004). The lower section of FA1 member conformably overlies Kharus Formation, deposited in a similar shallow-marine environment. The Fara Formation starts where the first beds of siliciclastic rocks occur. The lower part of FA1 contains slumps and breccias, indicating an unstable paleoslope. Some volcaniclastic beds were deposited during early FA1 times. We suggest that slope instability could be related to the onset of uplift during the deposition of FA1, accompanied by distal volcanism. Above the 15-m-thick base of ara Formation, silicilyte is the predominant lithology of FA1, with a thickness of ca. 90 m. This rock type reflects low deposition rates and water depth around 100-200 m (Amthor et al., 2005; Stolper et al., 2017). Thus, FA1 accumulated during basin deepening (Allen, 2011).

The culmination of a tectonic uplift, occurred during FA2 sedimentation, forming a relatively steep and unstable proximal slope (basin deepening) as advocated by the occurrence of slumps, massive breccias and neptunian dikes. The uplift was associated with proximal volcanism along an active continental margin, as revealed by samples NF1, NF2, changing from a passive margin to an active margin setting. The paleocurrents were consistently directed towards the SW, and thus, the area to the NE was necessarily exhumed and shed material in a probable NW/SE-extending basin.

The upper member of Fara Formation (FA3) consists of a heterogeneous, mostly clastic succession, with conspicuous volcaniclastic deposits at the base of FA3. Moreover, crossbedding, erosional surfaces and current ripple marks suggest a shallow ramp sedimentary environment affected by wave and current activities, receiving the sediments from a volcanic source area. Such was the paleoenvironment inhabited by the organism *Palaeopascichnus*. FA3 formed under stable tectonic conditions without uplift, sealing an angular unconformity between FA2 and FA3. However, volcanic layers at the bottom of FA3 indicate the occurrence of distal volcanism related with an active continental margin, based on the geochemical fingerprint of the studied volcaniclastic rocks. FA3 can be summarized as a sequence of fine-grained siliclastic rocks, including some volcaniclastic intercalations near the base. FA3 did not record any evidence of active tectonics/uplift during deposition. The wave ripples indicate high-energy conditions in a shallow marine setting (nearshore) as well as the current ripples (tidal influence). The suspension deposits represent tempestite (no turbidites) as there are only shallow marine indicators in FA3.

The existing unconformity between FA2 and FA3 members, and the fact that D1/F1 structures occur in FA1 and FA2 but not in FA3 members, demonstrates that D1 deformation had ceased in FA3. The shortening direction of D1 was NE/SW and correlates with the Cadomian Orogeny (Callegari et al., 2020). The arising Cadomian deformation affected the Jabal Akhdar area during the late Ediacaran at ca. 555 Ma (top Kharus Formation) to 547 Ma (dated volcanic rocks from the base FA2), but pre-dates 545-543 Ma (volcanic rocks from the FA3) if the U-Pb ages are taken at face values (see above). The 545-543 Ma-old volcanic rocks within FA3 member demonstrate that volcanism distal to Jabal Akhdar took place, although Cadomian deformation had ceased in that particular area.

Geodynamic Model

The medium- to high-K calc-alkaline signatures of the volcaniclastic rocks from Fara Formation resemble the geochemistry of similar-aged samples of the Hormuz region in Iran, formed during the Cadomian Orogeny (compare Farmarzi et al., 2015). Discrimination diagrams classify the samples from both Iran and Jabal Akhdar as having formed in an active continental margin setting (Fig. 16). Their geochemical signature and ages show that FA1 and FA2 rocks accumulated during the Cadomian Orogeny, which is also supported by the NE/SW-directed D1 shortening direction recorded in the pre-FA3 rocks of the Jabal Akhdar region (Figs. 18, 19).

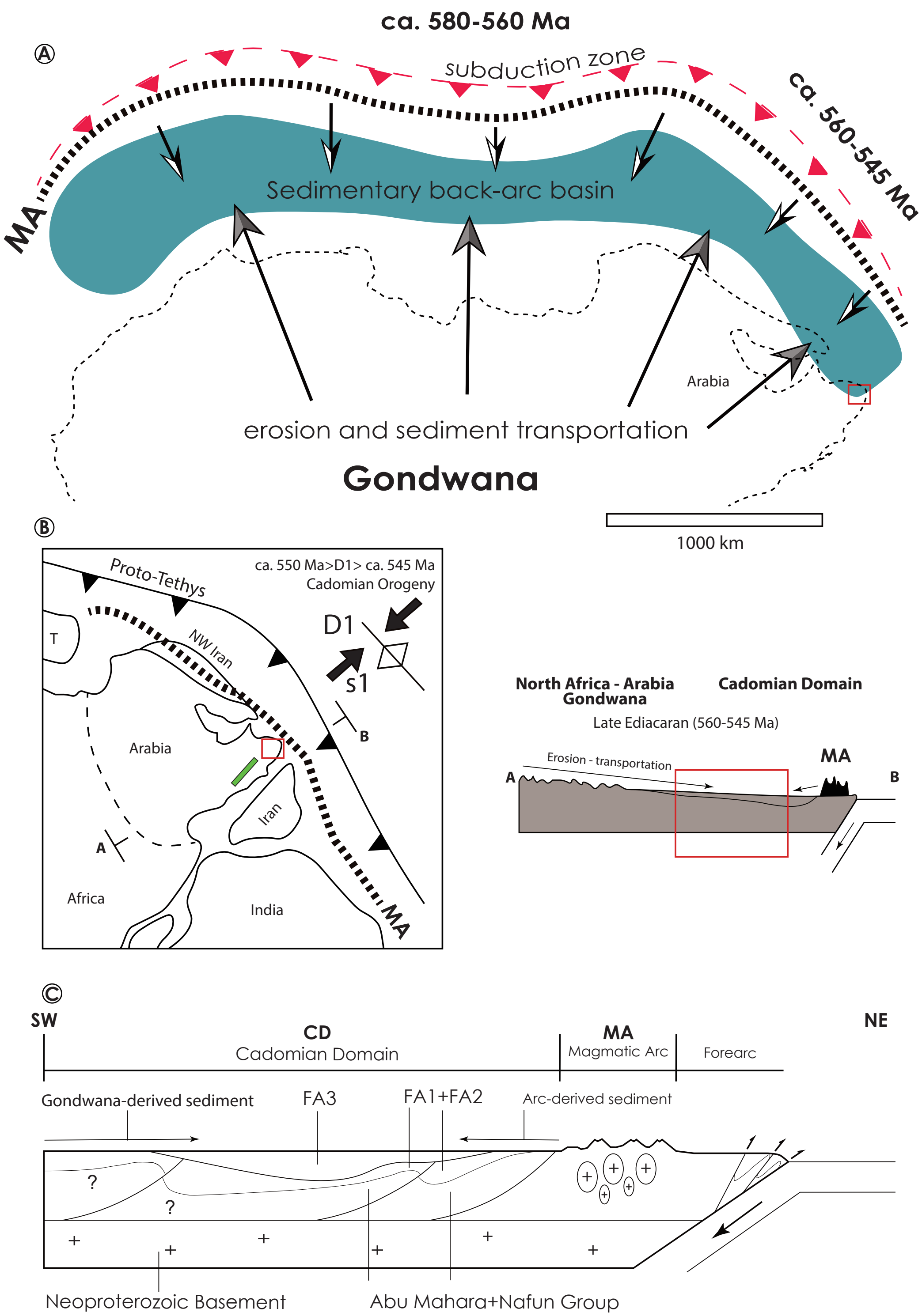

Figure 19. Geodynamic model for the Cadomian Orogeny of the study area. (a) – Cadomian Orogeny in northern Africa and Arabia (modified after Garfunkel, 2015). (b) left – Cadomian Orogeny (D1) in Arabia with shortening direction (s1) after Callegari et al. (2020). The green rectangle represents the Infra-Cambrian salt basins of the Ara Group. (b) right - Cross-section through the Cadomian Orogen and the Jabal Akhdar area.

(c) – Extended cross section of ('b'). Note that FA1 and FA2 are affected by Cadomian shortening, while FA3 seals it. MA=Magmatic Arc, CD=Cadomian Domain.

Our data confirms that rocks of the Ara Formation from south Oman (overall time-equivalent to Fara Formation) formed in a different paleo-tectonic setting than the Fara´s rocks. The lithologies of Ara accumulated in NNE-striking restricted intra-continental basins, while Fara´s filled the probably NW-striking continental back-arc basin. It is likely that NNE-striking faults at the margin of the NNE-striking basins were (re)activated as pull-apart basins during the Cadomian Orogeny, leading to basin deepening (green rectangle in Fig. 19b). Reactivation might be the expression of a non-coaxial stress field in the back-arc during subduction. The NNE-striking faults occur in northern Oman and formed during Pan-African terrain accretion (Weidle et al., 2022; 2023).

The onset of Cadomian deformation in the region of Jabal Akhdar triggered the development of a continental back-arc basin, alongside volcanism as recorded in FA1 member. At the same time, the slumps, breccias and siliciclastic input seen in the latter member illustrate the collapse of the former Kharus (Buah) carbonate ramp. Cadomian deformation in the Jabal Akhdar area postdates the ~550 Ma-old top Buah Formation in the Huqf area, providing we establish that Kharus Formation is the time equivalent of the Buah Formation (Cozzi et al., 2004). However, such deformation predates (~545 Ma, U-Pb zircon ages) the volcaniclastic rocks of the post-Cadomian basal FA3. The medium- to high-K calc-alkaline volcanism, distal to the Jabal Akhdar area, strengthens the interpretation of an ongoing Cadomian Orogeny, probably northeast of that area (Fig. 19).

SUMMARY/CONCLUSIONS

The ~412-m-thick Fara Formation of the Jabal Akhdar Dome consists of three members (FA1, FA2, FA3) with distinct sedimentary and structural features. FA1 indicates the onset of tectonic uplift and basin deepening, conformably overlying the shallow-marine carbonate ramp of the Kharus Formation. FA1 marks the transition from a passive to an active margin. FA2 contains an alternation of volcaniclastic rocks with a variety of sedimentary rocks, associated with the culmination of tectonic activity. FA3 consists mostly of shallow-marine siliciclastic rocks with some volcaniclastic material at its base. This upper member testifies stable tectonic conditions, also indicated by an angular unconformity between FA2 and FA3 (Cadomian Unconformity). Geochemical analyses and thin section petrography of volcanoclastic from FA2 and FA3 document that these rocks were strongly affected by hydrothermalism. Thus, the previously dated zircons from these rocks (547-543 Ma of Brasier et al., 2000; Bowring et al., 2007) are possibly older.

Geochemical analyses of FA2 and FA3 volcaniclastic rocks suggest that Fara Formation is tectonically linked to Hormuz Island in present-day Iran (compare Faramariz et al., 2015). Fara Formation was deposited within a continental back-arc basin during the Cadomian Orogeny. This correlation indicates that Fara Formation and the time-equivalent Ara Group of Interior Oman formed within distinct tectonic basins: Fara Formation in a NW-striking continental back-arc basin and Ara Group in a possible intracontinental pull-apart basin, which opened during the reactivation of Pan-African NNE-striking faults, during the Cadomian NE/SW-directed deformation field. Based on the stratigraphical, paleontological (*Palaeopascichnus linearis*, within FA3), structural, and geochemical data presented in this study, we propose that the age of the Fara Formation is entirely Ediacaran, i.e., >538 Ma (Cohen et al., 2013; updated 2023/06).

APPENDICES

Appendix 1 – Stratigraphic log description of Fara Formation with lithological and sedimentary features descriptions.

Appendix 2. -Areal distribution of the field work, continuous red lines represent the tracks of stratigraphic analysis for the realization of Logs 1-5, the coloured rectangles represent different area of field work carried out in different time with structural and stratigraphic analysis.

Appendix 3 – Whole rock analysis table

Appendix 4 - Legend of the geological cross sections.

ACKNOWLEDGEMENT

We thank Katharina Scharf for fieldwork assistance. The article improved by the constructive work of the reviewers and the Editor. This research did not receive any specific grant from funding agencies in the public, commercial, or not-for-profit sectors.

Author contributions

IC: Conceptualization, Formal Analysis, Investigation, Methodology, Visualization, Writing – Original Draft

AS: Formal Analysis, Investigation, Methodology, Visualization, Writing – Review & Editing

AFP: Formal Analysis, Investigation, Methodology, Visualization, Writing – Review & Editing

FM: Formal Analysis, Investigation, Methodology, Writing – Review & Editing

RM: Investigation, Writing – Review & Editing

DD: Investigation – Review & Editing

HR: Investigation

Data availability statements

All data generated or analysed during this study are available from the corresponding author on request.

REFERENCES

Agard, P., Searle, M.P., Alsop, G., Dubacq, B., 2010. Crustal stacking and expulsion tectonics during continental subduction: P-T deformation constraints from Oman. Tectonics 29, 1-19, doi: 10.1029/2010TC002669.

Al-Husseini, M.I., 2000. Origin of the Arabian Plate Structures: Amar Collision and Najd Rift. GeoArabia 5(4), 527-542.

Al-Kindy, M.H., Richard, P.D., 2014. The main structural styles of the hydrocarbon reservoirs in Oman. In: Rollinson, H.R., Searle, M.P., Abbasi. I.A., Al-Lazki, A.I., Al-Kindy, M.H. (Eds.), Tectonic evolution of the Oman Mountains. Geological Society, London, Special Publication, vol. 392(1), pp. 409-445, doi: 10.1144/SP392.20.

Allen, P.A., 2007. The Huqf Supergroup of Oman: Basin development and context for Neoproterozoic glaciation. Earth-Science Reviews 84, 139-185.

Allen, P.A., Leather, J., 2006. Post-Marinoan marine siliciclastic sedimentation: the Masirah Bay Formation, Neoproterozoic Huqf Supergroup of Oman. Precambrian Research 144, 167-198.

Allen, P.A., Leather, J., Brasier, M.D., Rieu, R., McCarron, M., Le Guerroué, E., Etienne, J.L., Cozzi, A., 2011. Chapter 20 The Abu Mahara Group (Ghubrah and Fiq formations), Jabal Akhdar, Oman. Geological Society, London, Memoirs 36, 251-262, doi: 10.1144/M36.20.

Al-Rawahi, H., Gomez-Perez, I., Bergmann, K., Cantine, M., Fonseca-Rivera, C., 2018. Sedimentology and Isotopes Stratigraphy of the Fara Formation in North Oman Outcrops and its Relation to the South Oman Subsurface. Seventh Arabian Plate Geology Workshop of the European Association of Geoscientists & Engineers: Pre-Cambrian to Early Paleozoic Petroleum Systems in the Arabian Plate, 9-13 December, Muscat, Oman

Al-Wardi, M., Butler, R.W.H., 2007. Constrictional extensional tectonics in the northern Oman mountains, its role in culmination development and the exhumation of the subducted Arabian continental margin. In: Ries, A.C., Butler, R.W.H., Graham, R.H. (Eds.), Deformation of the Continental Crust: The Legacy of Mike Coward. Geological Society, London, Special Publications, vol. 272, pp. 187-202.

Amthor, J.E., Grotzinger, J.P., Schröder, S., Bowring, S.A., Ramezani, J., Martin, M.W., Matter, A., 2003. Extinction of Clodina and Namacalathus at the Precambrian-Cambrian boundary in Oman. Geology 31(5), 431-434.

Amthor, J., Ramseyer, K., Faulkner, T., Lucas, P., 2005. Stratigraphy and sedimentology of a chert reservoir at the Precambrian-Cambrian Boundary: the Al Shomou Silicilyte, South Oman Salt Basin. GeoArabia 10(2), 89-122.

Béchennec, F., Roger, J., Le Métour, J., Wyns, R., 1992. Geological map of Seeb, sheet NF 40-03, scale 1:250,000, with Explanatory Notes: Directorate General of Minerals, Oman Ministry of Petroleum and Minerals.

Beurrier, M., Béchennec, F., Rabu, D., Hutin, G., 1986. Geological map of Rustaq, sheet NF 40-03D, scale 1:100,000, with Explanatory notes: Directorate General of Minerals, Oman Ministry of Petroleum and Minerals.

Blendinger, W., van Vliet, A.T., Hughes Clarke, M.W., 1990. Updoming, rifting and continental margin development during the Late Paleozoic in northern Oman. In: Robertson, A.H.F., Searle, M.P., Ries, A.C. (Eds.), The Geology and Tectonics of the Oman Region. Geological Society of London, Special Publication, vol. 49, pp. 27-37.

Bowring, S.A., Grotzinger, J.P., Condon, D.J., Ramezani, J., Newall, M., Allen, P.A., 2007. Geochronologic constraints of the chronostratigraphic framework of the Neoproterozoic Huqf Supergroup, Sultanate of Oman. American Journal of Science 307, 1097-1145, doi: 10.2475/10.2007.01.

Brasier, M., McCarron, G., Tucker, R., Leather, J., Allen, P., Shields, G., 2000. New U-Pb zircon dates for the Neoproterozoic Ghubrah glaciation and for the top of the Huqf Supergroup, Oman. Geology 28(2), 175-178.

Breton, J.-P., Béchennec, F., Le Métour, J., Moen-Maurel, L., Razin, P., 2004. Eoalpine (Cretaceous) evolution of the Oman Tethyan continental margin: insights from a structural field study in Jabal Akhdar (Oman Mountains). GeoArabia 9(2), 41-58.

Callegari, I., Scharf, A., Mattern, F., Bauer, W., Pinto, A.J., Scharf, K., Rarivoarison, H., Al-Kindi, M.H., 2020. Gondwana accretion tectonics and implications for the geodynamic evolution of eastern Arabia: first structural evidence of the existence of the Cadomian Orogeny in Oman (Jabal Akhdar Dome, Central Oman Mountains). Journal of Asian Earth Sciences 187, 104070, doi: 10.1016/j.jseaes.2019.104070.

Chauvet, F., Dumont, T., Basile, C., 2009. Structures and timing of Permian rifting in the central Oman Mountains (Saih Hatat). Tectonophysics 475, 563-574, doi: 10.1016/j.tecto.2009.07.008.

Cohen, K.M., Finney, S.C., Gibbard, P.L. & Fan, J.-X. (2013; updated v2023/06). The ICS International Chronostratigraphic Chart. Episodes 36: 199-204.

Cozzi, A., Grotzinger, J.P., Allen, P.M., 2004. Evolution of a terminal Neoproterozoic carbonate ramp system (Buah Formation, Sultanate of Oman): Effects of basement paleotopography. Geological Society of America Bulletin 116(11-12), 1367-1384, doi: 10.1130/B25387.1.

Cozzi, A., Rea, G., Craig, J., 2012. From global geology to hydrocarbon exploration" Ediacaran –Early Cambrian petroleum plays of India, Pakistan and Oman. Geological Society, London, Special Publications 366, doi: 10.1144/SP366.14.

Droste, H., 2014. Petroleum geology of the Sultanate of Oman. In: Marlow, L., Kendall, C., Yose, L. (Eds.), Petroleum Systems of the Tethyan Region. American Association of Petroleum Geologists Memoir 106, 713-755, doi: 10.1036/12431870M1063039.

Dong, L., Xiao, S., Shen, B., Zhou, C., 2008. Silicified Horodyskia and Palaeopascichnus from upper Ediacaran cherts in South China: tentative phylogenetic interpretation and implications for evolutionary stasis. Journal of the Geological Society 165, 367–378.

Edgell, H.S., 1991. Proterozoic salt basins of the Persian Gulf area and their role in hydrocarbon generation. Precambrian Research 54, 1-14.

El-Ghali, M., Hersi, O., Abbasi, I., 2020. Direct in-situ U-Pb carbonate geochronology of the Late Neoproterozoic Kharus Formation, Jabal Akhdar, Northern Oman. The 13th International Geological Conference SSG2020, Jeddah, Saudi-Arabia.

Faqira, M., Rademakers, M., Afifi, A., 2009. New insights into the Hercynian Orogeny, and their implications for the Paleozoic Hydrocarbon System in the Arabian Plate. GeoArabia 14(3), 199-228.

Faramarzi, N. G., Amini, S., Schmitt, A. K., Hassanzadeh, J., Borg, G., McKeegan, K., Razavi, S. M. H., Mortazavi, S. M., 2015. Geochronology and geochemistry of rhyolites from Hormuz Island, southern Iran: A new record of Cadomian arc magmatism in the Hormuz Formation. Lithos 236-237, 201-211.

Forbes, G.A., Jansen, H.S.M., Schreurs, J., 2010. Lexicon of Oman subsurface stratigraphy. Reference guide to the stratigraphy of Oman's Hydrocarbon basins. GeoArabia, Special Publication 5 by Gulf Petro Link, p. 373.

Garfunkel, Z., 2015. The relations between Gondwana and the adjacent peripheral Cadomian domain—constrains on the origin, history, and paleogeography of the peripheral domain. Gondwana Research 28, 1257–1281.

Glennie, K.W., Boeuf, M.G.A., Hughes Clarke, M.W., Moody-Stuart, M., Pilaar, W., Reinhardt, B.M. 1974. Geology of the Oman Mountains. Koninklijk Nederlands Geologisch en Mijnbouwkundig Genootschap, Transactions 31(1), p. 423.

Gorton, M.P., Schandl, E.S., 2000. From continents to island arcs: a geochemical index of tectonic setting for arc-related and within-plate felsic to intermediate volcanic rocks. Canadian Mineralogist 38, 1065-1073.

Grobe, A., Virgo, S., von Hagke, C., Urai, J.L., Littke, R., 2018. Multiphase structural evolution of a continental margin during obduction orogeny: Insights from the Jebel Akhdar Dome, Oman Mountains. Tectonics 37(3), 888-913, doi: 10.1002/2016TC004442.

Grobe, A. von Hagke, C., Littke, R., Dunkl, I., Wübbeler, F., Muchez, P., Urai, J.L., 2019. Tectono-thermal evolution of Oman's Mesozoic passive continental margin under the obducting Semail Ophiolite: a case study of Jebel Akhdar, Oman. Solid Earth 10, 149-175, doi: 10.5194/se-10-149-2019.

Grotzinger, J., Al-Rawahi, Z., 2014. Depositional facies and platform architecture of microbialite-dominated carbonate reservoirs, Ediacaran-Cambrian Ara Group, Sultanate of Oman. AAPG Bulletin 98(8), 1453-1494, doi: 10.1306/02271412063.

Hansman, R.J., Ring, U., Thomson, S.N., den Brock, B., Stübner, K., 2017. Late Eocene uplift of the Al Hajar Mountains, Oman, supported by stratigraphic and low-temperature thermochronology. Tectonics 36(12), 3081-3109, doi: 10.1002/2017TC004672.

Hansman, R.J., Ring, U., Scharf, A., Glodny, J., Wan, B., 2021. Structural architecture and Late Cretaceous exhumation history of the Saih Hatat Dome (Oman), a review based on existing data and semi-restorable cross-sections. Earth-Science Reviews 217, 103595, doi: 10.1016/j.earscirev.2021.103595.

Heward, A.P., Miller, C.G., Booth, G.A., 2018. The Early Ordovician Middle Shale Member (Am3) of the Amdeh Formation and further evidence of conodont faunas from the Sultanate of Oman. Geological Magazine 156, 1357–1374.

Heward, A.P., Penney, R.A., 2014. Al Khlata glacial deposits in the Oman Mountains and their implications. In: Rollinson, H.R., Searle, M.P., Abbasi, I., Al-Lazki, A. Al-Kindy, M.H. (Eds.), Tectonic Evolution of the Oman Mountains, Geological Society, London, Special Publication, vol. 392(1), pp. 279-301, doi:10.1144/SP392.15.

Immerz, P.W., Oterdoom, H., El-Tonbary, M., 2000. The Huqf/Haima hydrocarbon system of Oman and the termianl phase of the Pan-African Orogeny: Evaporite depositions in a compressive setting. 4th Middle East Geosciences Conference, GEO 2000, GeoArabia, Abstract 5(1), 113-114.

Kolesnikov, A.V., Rogov, V.I., Bykova, N.V., Danelian, T., Clausen, S., Maslov, A.V., Grazhdankin, D.V., 2018. The oldest skeletal macroscopic organism Palaeopascichnus linearis. Precambrian Research 316, 24–37.

Koopman, A., van der Berg, M., Romine, K., Teasdale, J., 2007. Proterozoic to Cambrian plate-tectonics and its control on the structural evolution of the Ara Salt-Basin in Oman. Abstract AAPG European Region Conference, Athens, Greece: AAPG Search and Discovery Article #90072.

Loosveld, R.J.H., Bell, A., Terken, J.J.M., 1996. The tectonic evolution of interior Oman. GeoArabia 1(1), 28-51.

Lovelock, P.E.R., Potter, T.L., Walswoth-Bell, E.B., Wiemer, W.M., 1981. Ordovician rocks in the Oman mountains: the Amdeh Formation. Geologie en Minjbouw 60, 487-495.

Mallard, L. D., & Rogers, J. J. (1997). Relationship of Avalonian and Cadomian terranes to Grenville and Pan-African events. Journal of Geodynamics, *23*(3-4), 197-221.

Mattern, F., Pracejus, B., 2018. Heavy mineral beach placers of the Ordovician Amdeh Formation (Member 4, Wadi Qahza, Saih Hatat, eastern Oman Mountains): Where is the main source area? Journal of African Earth Sciences 147, 633-646, doi.org/10.1016/j.jafrearsci.2018.06.031.

Mattern, F., Scharf, A., 2019. Transition from the Hajir Formation to the Muaydin Formation: A facies change coinciding with extensional, syndepositional faulting (Ediacaran, Jabal Akhdar Dome, Central Oman Mountains). Journal of African Earth Sciences 152, 237-244, doi.org/10.1016/j.jafrearsci.2019.02.016.

Mattes, B.W., Conway Morris, S., 1990. Carbonate/evaporate deposition in the Late Precambrian – Early Cambrian Ara Formation of Southern Oman. In: Robertson, A.H.F., Searle, M.P., Ries, A.C. (Eds.), The Geology and Tectonics of the Oman Region. Geological Society of London, Special Publication, vol. 49, pp. 617-636.

McCarron, G.M., 1999. Sedimentology and stratigraphy of the Nafun Group: Huqf Supergroup, Oman. Ph.D. thesis, Trinity College, Dublin, Ireland, Oxford University, p. 302.

McDonough, W. F., Sun, S. S., 1995. The composition of the Earth. Chem. Geol. 120, 223-253.

Mount, V.S., Crawford, R.I.S., Bergman, S.C., 1998. Regional Structural style of the Central and Southern Oman Mountains: Jabal Akhdar, Saih Hatat and the Northern Ghaba Basin. GeoArabia 3(4), 475-490.

Nicholas, C.J., Brasier, M., 2000. Outcrop equivalent of the subsurface Precambrian-Cambrian Ara Group in Oman. 4th Middle East Geosciences Conference, GEO 2000, GeoArabia, Abstract 5(1), 151-152.

Osburn, M., Grotzinger, J., Bergmann, K., 2014. Facies, stratigraphy, and evolution of a middle Ediacaran carbonate ramp: Khufai Formation, Sultanate of Oman. AAPG Bulletin 98(8), 1631-1667, doi: 10.1306/07291312140.

Oterdoom, W.H., Worthing, M.A., Partington, M., 1999. Petrological and tectonostratigraphical evidence for a Mid Ordovician rift pulse on the Arabian Peninsula. GeoArabia 4, 476-500.

Pearce, J.A. (1983) Role of the sub-continental lithosphere in magma genesis at active continental margins. In: Hawkesworth, C.J. and Norry, M.J. (Eds.) Continental Basalts and Mantle Xenoliths, Shiva Publishing Ltd., Cambridge, Mass., 230-249.

Peters, J.M., Filbrandt, J.B., Grotzinger, J.P., Newall, M.J., Shuster, M.W., Al-Siyabi, H.A., 2003. Surface-piercing salt domes of interior North Oman, and their significance for the Ara carbonate 'stringer' hydrocarbon play. GeoArabia 8(2), 231-270.

Pinto, A. J., Sanchez-Pastor, N., Callegari, I., Pracejus, B., Scharf, A., 2020. Challenges to rutile-based geoscientific tools: low-temperature polymorphic TiO_2 transformations and corresponding reactive pathways. Scientific Reports 10, 7445.

Rieu, R., Allen, P.A., Cozzi, A., Kosler, J., Bussy, F., 2007. A composite stratigraphy for the Neoproterozoic Huqf Supergroup of Oman: integrating new litho-, chemo- and chronostratigraphic data of the Mirbat area southern Oman. Journal of the Geological Society, London 164, 997-1009, doi: 10.1144/0016-76492006-114.

Rioux, M., Garber, J., Bauer, A., Bowring, S., Searle, M.P., Kelemen, P., Hacker, B., 2016. Synchronous formation of the metamorphic sole and igneous crust of the Semail ophiolite: New constraints on the tectonic evolution during ophiolite formation from high-precision U-Pb zircon geochronology. Earth and Planetary Science Letters 451, 185-195, doi: 10.1016/j.epsl.2016.06.051.

Scharf, A., Mattern, F., Pracejus, B., 2019. Two new microscopic ductile kinematic indicators from the Oman Mountains. Journal of Structural Geology 119, 107-117.

Scharf, A., Callegari, I., Mattern, F., Scharf, K., Carminati, E., 2021a. Triple folded surface morphology of Neoproterozoic rocks (Jabal Akhdar Dome, Oman Mountains) – insights into buttressing effects and regional tectonics. Journal of Asian Earth Sciences 221, 104942.

Scharf, A., Mattern, F., Al-Wardi, M., Frijia, G., Moraetis, D., Pracejus, B., Bauer, W., Callegari, I., 2021b. Tectonostratigraphy of the eastern part of the Oman Mountains. Geological Society, London, Memoirs, M54(1), 11-47, doi: 10.1144/M54.2.

Scharf, A., Mattern, F., Al-Wardi, M., Frijia, G., Moraetis, D., Pracejus, B., Bauer, W., Callegari, I., 2021c. Tectonic evolution of the Oman Mountains. Geological Society, London, Memoirs, M54(1), 67-103, doi: 10.1144/M54.5.

Schröder, S., Schreiber, B.C., Amthor, J.E., Matter, A., 2003. A depositional model for the terminal Neoproterozoic-Early Cambrian Ara Group evaporites in south Oman. Sedimentology 50, 879-898, doi: 10.1046/j.1365-3091.2003.00587.x.

Schröder, S., Grotzinger, J.P., 2007. Evidence for anoxia at the Ediacaran-Cambrian boundary: the record of redox-sensitive trace elements and rare earth elements in Oman. Journal of the Geological Society, London 164(1), 175-187, doi: 10.1144/0016-76492005-022.

Searle, M.P., 2007. Structural geometry, style and timing of deformation in the Hawasina Window, Al Jabal al Akhdar and Saih Hatat culminations, Oman Mountains. GeoArabia 12(2), 99-130.

Stampfli, G.M., Borel, G.D., 2002. A plate tectonic model for the Paleozoic and Mesozoic constrained by dynamic plate boundaries and restored synthetic oceanic isochrons. Earth and Planetary Science Letters 196, 17-33.

Stolper, D.A., Love, G.D., Bates, S., Lyons, T.W., Young, E., Sessions, A.L., Grotzinger, J.P., 2017. Paleoecology and paleoceanography of the Athel silicilyte, Ediacaran-Cambrian boundary, Sultanate of Oman. Geobiology 15, 401-426, doi: 10.1111/gbi.12236.

Styles, M.T., Ellison, R.A., et al., 2006. The Geology and Geophysics of the United Arab Emirates, vol. 2. Ministry of Energy, United Arab Emirates, Abu Dhabi.

Sun, S.S. and McDonough, W. F., 1989. Chemical and isotopic systematics of oceanic basalts: implications for mantle composition and processes. In: Saunders, A. D. and Norry, M. J. (Eds.) Magmatism in ocean basins. Geological Society of London Special Publication 42, 313-345.

Thomson, D., Rainbird, R.H., Krapez, B., 2015. Sequence and tectonostratigraphy of the Neoproterozoic (Tonian-Cryogenian) Amundsen Basin prior to supercontinent (Rodinia) breakup. Precambrian Research 263, 246–259.

Tilton, G.R., Hopson, C.A., Wright, J.E., 1981. Uranium-lead isotopic ages of the Semail ophiolite, Oman, with applications to Tethyan oceanic ridge tectonics. Journal of Geophysical Research 86(B4), 2763-2775.

Veevers, J.J., 2004. Gondwanaland from 650–500 Ma assembly through 320 Ma merger in Pangea to 185–100 Ma breakup: supercontinental tectonics via stratigraphy and radiometric dating. Earth-Science Reviews 68, 1–132. https://doi.org/10.1016/j.earscirev.2004.05.002

Weidle, C., Wiesenberg, L., El-Sharkawy, A., Krüger, F., Scharf, A., Agard, P., Meier, T., 2022. A 3-D crustal shear-wave velocity model and Moho map below the Semail Ophiolite, eastern Arabia. Geophysical Journal International 231(2), 817-834, doi: 10.1093/gji/ggac223.

Weidle, C., Wiesenberg, L., Scharf, A., Agard, P., El-Sharkawy, A., Krüger, F., Meier, T., 2023. Lithospheric evolution of eastern Arabia based on surface wave and receiver function analyses. Earth and Planetary Science Letters 611, 118145, doi: 10.1016/j.epsl.2023.118145.

Xiao, S., Kaufman, A.J. (Eds.), 2006. Neoproterozoic Geobiology and Paleobiology, Topics in Geobiology. Springer Netherlands, Dordrecht. https://doi.org/10.1007/1-4020-5202-2

Zuccari, C., Vignaroli, G., Callegari, I., Nestola, F., Novella, D., Giuntoli, F., Guillong, M., Viola, G., 2023. Forming and preserving aragonite in shear zones: First report of blueschist facies metamorphism in the Jabal Akhdar Dome, Oman Mountains. Geology.